

Original Article

Cite this article: Cardenas-Vera A, Lentz DR, McFarlane CRM, and Thorne KG (2023) Geochemistry, U-Pb geochronology and Nd-Hf isotopes of leucocratic dykes in the Cape Spencer area, southern New Brunswick, Canada: insights into the Alleghanian orogeny in the northern Appalachians. *Geological Magazine* **160**: 2129–2146. <https://doi.org/10.1017/S0016756824000141>

Received: 23 August 2023

Revised: 19 April 2024

Accepted: 28 April 2024

First published online: 23 September 2024

Keywords:


Albitite; Aplite; Monazite geochronology; Nd-Hf isotopes

Corresponding author:

Alan Cardenas-Vera;

Email: alan.cardenas@unb.ca

Geochemistry, U-Pb geochronology and Nd-Hf isotopes of leucocratic dykes in the Cape Spencer area, southern New Brunswick, Canada: insights into the Alleghanian orogeny in the northern Appalachians

Alan Cardenas-Vera¹ , David R. Lentz¹, Christopher R.M. McFarlane¹ and Kathleen G. Thorne²

¹Department of Earth Sciences, University of New Brunswick, Fredericton, NB, Canada and ²Geological Surveys Branch, New Brunswick Department of Natural Resources and Energy Development, Fredericton, NB, Canada

Abstract

Contrary to the southern Appalachians, where Alleghanian magmatism is widespread and well documented, the expressions of magmatism in the Canadian Appalachians are limited. In this study, a suite of leucocratic dykes from the Cape Spencer area in southern New Brunswick, Canada, were investigated to determine the nature, timing and source of these magmas using zircon and monazite U-Pb geochronology, whole-rock geochemistry and Nd-Hf isotopes. An LA-ICP-MS U-Pb monazite Alleghanian age of 273.7 ± 1.3 Ma obtained for these dykes constitutes a new example of magmatism in the northern segment of the orogen, where significant strike-slip movement and reheating have been the primary markers of the Alleghanian Orogeny. These metaluminous leucocratic dykes are enriched in light rare elements, U and Th; depleted in high-field strength elements (HFSE; Nb, P, Ti); and have slight negative Europium anomalies [$(Eu/Eu^*)_N = 0.72-0.95$]. All the dykes samples have negative $\epsilon Nd(t)$ values (-9.76 to -5.7), negative $\epsilon Hf(t)$ values (-1.8 to -1.0) and Mesoproterozoic Nd depleted-model ages ($T_{DM} = 1371-1618$ Ma). The geochemical and isotopic characteristics suggest that the dykes were formed by the partial melting of lower crust that assimilated Meguma metasedimentary rocks and/or Avalonian sedimentary rocks, following terminal subduction of the Rheic Ocean and thermal re-equilibration during the Alleghanian orogeny. The effects of the closure of the Rheic Ocean in the oblique collision between composite Laurentia and Gondwana were, to a certain extent, accommodated along the Minas Fault Zone, where magmatism and regional fluid flow were concentrated.

1. Introduction

The deformation history in the northern Appalachians (southern New England through Atlantic Canada) during the Carboniferous is associated mainly with the docking and adjustment of the Meguma terrane to composite Laurentia along the Minas Fault Zone (MFZ) (Murphy *et al.* 2011; van Staal & Barr, 2012; Park *et al.* 2014; Waldron *et al.* 2015; Park & Hinds, 2020). This Carboniferous-Permian (330–260 Ma) deformation, also referred to as the Alleghanian orogeny, constitutes the final stage of oceanic closure by the collision of Africa with composite Laurentia to form the supercontinent Pangea (Hatcher, 2002). Late Paleozoic magmatism is well known and widespread in the southern Appalachians, where over 60 Alleghanian plutons have been documented in contrast to very limited magmatism in the northern segment of the orogen (Samson *et al.* 1995; Speer & Hoff, 1997; Hatcher, 2005; Hibbard *et al.* 2007a, 2010). The nearest Alleghanian intrusions to the Cape Spencer area are the Bank German pluton (Pe-Piper & Jansa, 1999; Pe-Piper *et al.* 2010), in the southwestern end of the Scotian Shelf, approximately 30 km southwest of Yarmouth, Nova Scotia (Canada), and the Sebago batholith and granitic pegmatites from New England (USA) (Tomascak *et al.* 1996a, 1996b, 1998). The Alleghanian orogeny, in the context of the Canadian Appalachians, is palpable by major strike-slip movements along the MFZ (Murphy & Keppie, 1998; Murphy *et al.* 2011; Waldron *et al.* 2015) and localized thermal and magmatic events restricted to or in the periphery of shear zones (Kontak *et al.* 2000, 2008; MacHattie & O'Reilly, 2008; Pe-Piper *et al.* 2010, 2018). In this context, a group of leucocratic dykes have been described as intruding on the rocks in the Cape Spencer area and they also crosscut the deformational fabrics of the host rocks (Warner, 1985; Nance, 1986; Nance & Warner, 1986), although have not been comprehensively studied. These bodies constitute an opportunity to provide an upper age constraint to the fabrics related to the deformation episode and the gold mineralization event (Watters, 1993; Richard, 2005) linked to these ductile to brittle fabrics. A lower constraint is already given by the

© The Author(s), 2024. Published by Cambridge University Press. This is an Open Access article, distributed under the terms of the Creative Commons Attribution licence (<http://creativecommons.org/licenses/by/4.0/>), which permits unrestricted re-use, distribution and reproduction, provided the original article is properly cited.



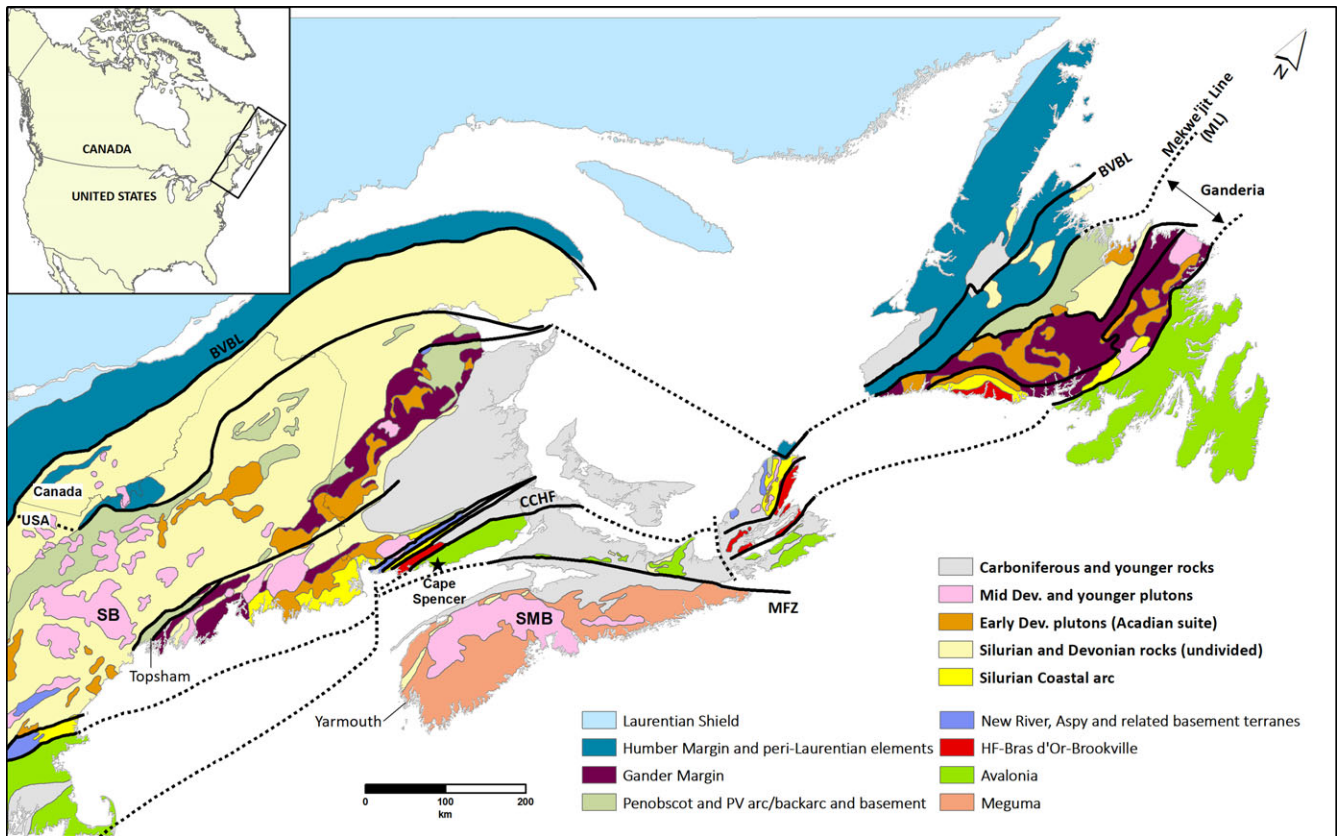


Figure 1. (Colour online) Simplified lithotectonic division of the northern Appalachians. CCHF: Caledonia-Clover Hill Fault. MFZ: Minas Fault Zone. BVBL: Baie Verte Brompton Line. ML: Mekwe'jit Line (formerly Red Indian Line; RIL). SB: Sebago Batholith. SMB: South Mountain Batholith. Modified after van Staal *et al.* (2021).

age of the youngest unit affected by this deformation, i.e. the Lancaster Formation, which is considered Bashkirian (Park & Hinds, 2020). In this study, the petrographical, whole-rock geochemical, U-Pb zircon and monazite geochronological characteristics, and Nd-Hf isotopic composition of the leucocratic dykes outcropping in the Cape Spencer area in southern New Brunswick, are presented to provide constraints on their petrogenesis and significance within the geological framework of the northern Appalachians and its tectonomagmatic evolution during the Alleghanian orogeny.

2. Geological overview

2.a. Regional geology

The northern Appalachians (Figure 1) developed through a long-term process of accretion and collision of peri-Laurentian and peri-Gondwanan (Ganderia, Avalonia, and Meguma) terranes to the Laurentian continental margin during the closure of the Iapetus and Rheic oceans between the late Cambrian and the Permian (Hibbard *et al.* 2007b; van Staal, 2007; Hatcher, 2010; Waldron *et al.*, 2019). The Alleghanian orogeny includes all the events related to the collision/amalgamation of composite Laurentia with Gondwana (Hatcher, 2010; van Staal & Barr, 2012); this collision, in the northern Appalachians, was dominated by dextral-strike-slip motion along the MFZ (Murphy *et al.* 2011). However, the effects of the Alleghanian orogeny are not restricted to the MFZ, with Alleghanian deformation through fault movement documented in the Gaspé Peninsula of Quebec (Jutras *et al.* 2003),

Ar-Ar resetting around 270–300 Ma in shear zones in the southern Meguma terrane and associated offshore plutons (Reynolds *et al.* 2012), in addition to shear zones formation (~320 Ma) north of Yarmouth (Culshaw & Reynolds, 1997).

The Caledonia-Clover Hill Fault in New Brunswick marks the boundary between Ganderia and Avalonia (Park *et al.* 2014; Waldron *et al.* 2015). Avalonia describes a distinctive group of Neoproterozoic, arc-related, volcano-sedimentary sequences and plutonic rocks (Kerr *et al.*, 1995; van Staal, 2007). The Caledonia terrane, i.e. a segment of Avalonia in southern New Brunswick, includes three Cryogenian to Ediacaran volcanic-sedimentary sequences and comagmatic intrusions (Pollock *et al.* 2022; Waldron *et al.* 2022), the recently recognized ca. 690 Ma Lumsden Group, the ca. 630–615 Ma Broad River Group and the ca. 560–550 Ma Coldbrook Group (Barr & White, 1996a, 1996b, 1999; Barr *et al.* 2019; Barr *et al.* 2020; Johnson & Rossiter, 2022) (Figure 2(a)). These sequences are overlain by Cambrian to Early Ordovician sedimentary rocks of the Saint John Group, and several other Carboniferous and Triassic successions (Tanoli & Pickerill, 1988; Landing, 1996; Fyffe *et al.* 2011). The Lumsden Group is characterized by chert and tuffaceous siltstone, intermediate crystal and lithic tuff, felsic volcanic rocks and associated plutons (Johnson & Rossiter, 2022). The Broad River Group includes intermediate and felsic crystal lithic tuff, mafic and felsic flows and associated plutons, tuffaceous sedimentary rocks, arkosic sandstone and conglomerate that have experienced regional metamorphism to greenschist facies along with ductile deformation (Barr & White, 1996a). The Coldbrook Group consists of a first group of dacitic and rhyolitic flows and tuffs, and

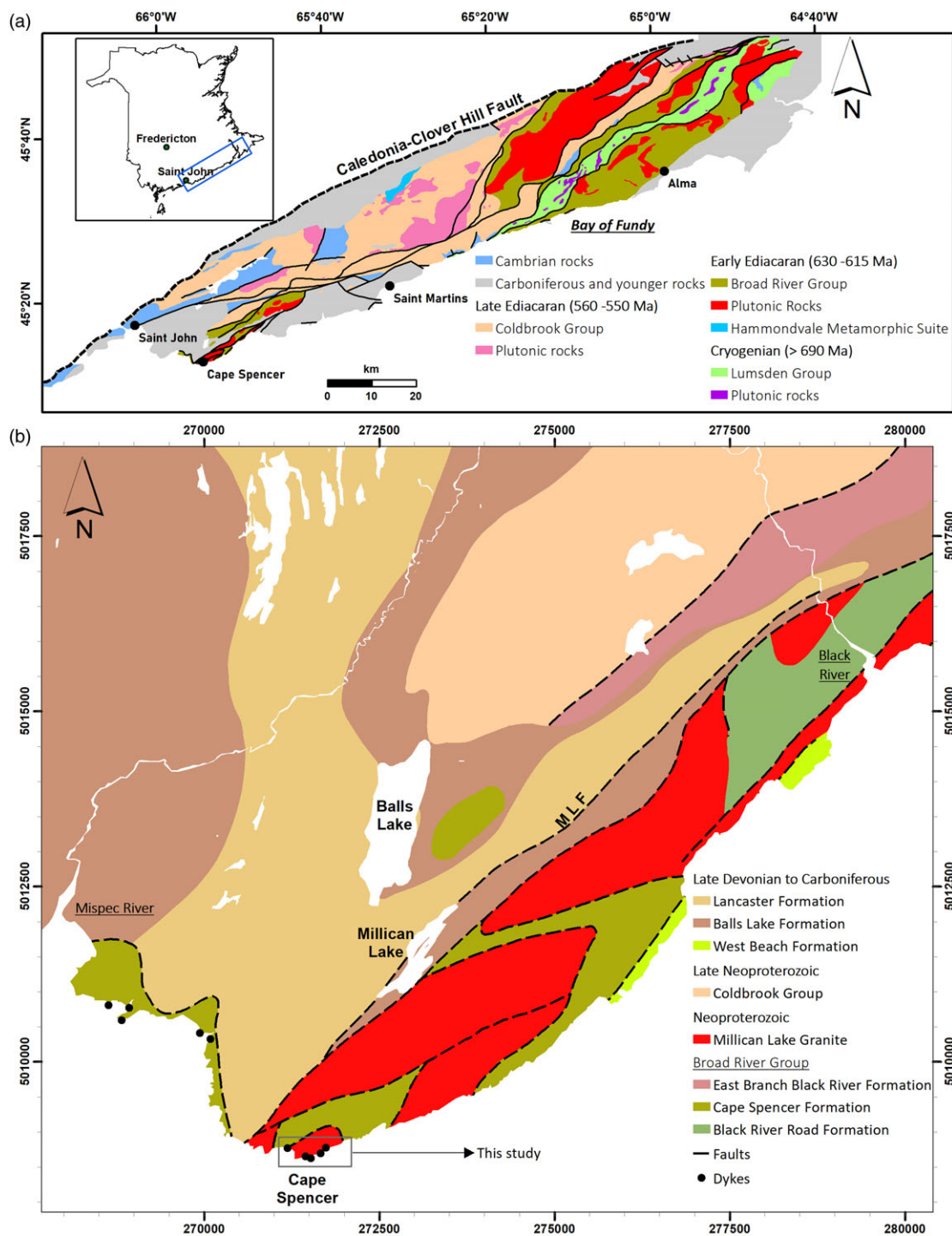


Figure 2. (Colour online) (a) Simplified geological map of the Caledonia Highlands. Modified from Barr and White (1999). (b) Local geology of the Cape Spencer area. Modified from Watters (1993) and the bedrock geological compilation of the Cape Spencer area, maps National Topographic Series 21H/04 and 21H/05 (2004).

a second group of basaltic and rhyolitic units along with coarse clastic sedimentary rocks and comagmatic plutons, considered to be less deformed and metamorphosed than the Broad River Group (Barr & White, 1999). The petrological characteristics of the igneous components of both the Lumsden and Broad River groups suggest an origin in a continental margin subduction zone, whereas the Coldbrook Group, because of its bimodal nature, is thought to have formed during extension after cessation of continental arc magmatism (Barr & White, 1999; Pollock *et al.* 2022).

The MFZ marks the boundaries between Avalonia and the Meguma terrane (Williams, 1979; Murphy *et al.* 2011). The Meguma terrane, the most outboard of the Appalachian terranes in Canada, derived from the West African craton (Clarke & Halliday, 1985; Waldron *et al.* 2009; White & Barr, 2010; White *et al.* 2018), constitutes a succession of Cambrian-Ordovician turbiditic sediments of the Goldenville and Halifax groups and mid to late Devonian granitoids that include the South Mountain Batholith (Clarke *et al.* 1997, 2004; White, 2010).

2.b. Local geology

The Cape Spencer area is located 15 km southeast of Saint John, New Brunswick, within the Caledonia terrane, representing a segment of Avalonia in southern New Brunswick (Barr *et al.* 2020). The Cape Spencer area presents polyphase fold-and-thrust style deformation of the rock units (Nance & Warner, 1986; Nance, 1987) and is centred along the Millican Lake Fault, a NE-SW striking fault (Figure 2(b)). The lithological units present in the area include mainly mafic volcanic rocks and a lesser amount of felsic volcanic rocks of the Coldbrook Group, and rocks of the Millican Lake Granite, a name used to refer to a group of highly sheared intrusions consisting of granite, granodiorite and leucogranite with a U-Pb (zircon) age of 623 ± 2 Ma (Watters, 1993). These units commonly share thrust-faulted contacts with the purple/grey siltstone, slate, coarse-grained polymictic conglomerate and granite-cobble conglomerate of the Cape Spencer Formation (Watters, 1993; Barr & White, 1999). Given the unclear relationship between the Cape Spencer Formation and the Millican Lake Granite, the age of the former remains ambiguous. However, Barr and White (1999) included it in the Broad River Group based on the similarity of some components shared by the clastic units.

The reddish-brown quartz-pebble conglomerate, medium-grained sandstone and shale of the Balls Lake Formation (Viséan-Serpukhovian) are faulted against both the underlying Cape Spencer Formation and the overlying grey quartzose sandstone and siltstone, shale and conglomerate of the Lancaster Formation (Bashkirian) (Watters, 1993; Park & Hinds, 2020). The West Beach Formation includes intensely deformed basalt with grey shale and siltstone interbeds (Park *et al.* 2014).

Watters (1993) described the presence of two main deformation phases in the Cape Spencer area: an early deformation D_1 , produced folds (F_1), verging to the NW with a pressure-solution cleavage (S_1) dipping to the SE-SSE. The succeeding phase of deformation, D_2 , produced conjugate SE- and NW-dipping thrust faults and a late minor set of folds (F_2), overturned to the SE-SSE with a cleavage (S_2) dipping to the NW-NNW that crenulates S_1 . The area is dominated by thrusts and reverse faults associated with the F_1 folds and S_1 cleavage, in addition to NW-dipping reverse faults offsetting both the F_1 folds and associated thrusts (Nance, 1986; Watters, 1993). The overprinting relationships of folds and cleavage, including reversed overprinting geometries, suggest near-contemporaneous events (Park & Hinds, 2020). Gold mineralization occurs along strongly faulted and sheared lithological contacts between the Millican Lake Granite and the Cape Spencer Formation within pyrite-rich portions of illitized (illite-carbonate \pm quartz \pm pyrite \pm specularite) zones (Ruitenberg, 1995) localized along D_2 thrust faults and folds. The gold is associated with quartz \pm carbonate \pm plagioclase \pm sulphide (pyrite, chalcopyrite) \pm specularite veins that vary from several millimetres to several decimetres in width that parallel the folded S_1 cleavage and (or) the S_2 cleavage (Watters, 1993). The deformational fabrics associated with gold mineralization are crosscut by aplitic sill-like masses and smaller dykes, and are the focus of this study (Warner, 1985; Nance, 1986).

3. Material and methods

3.a. Sampling and element analyses

Ten representative samples of the dykes were selected for petrological and geochemical analyses around the Cape Spencer area, following detailed field investigations and sample collection.

Polished thin sections of the rocks were prepared at the University of New Brunswick. The geochemical analyses were performed on fresh and representative samples by Activation Labs (Actlabs) in Ancaster, Ontario that were crushed and split to 0.5 kg, then pulped in a ceramic mill. They were then analysed using lithium borate fusion inductively coupled plasma-optical emission spectrometry (ICP-OES) and mass spectrometry (ICP-MS) for major- and trace-element analyses, respectively. Analytical uncertainties using these techniques are less than 1%. Elements such as Au, As, Br, Cr, Ir, Sc, Se and Sb were analyzed by Instrumental Neutron Activation Analysis. Quality assurance and quality control procedures, including the use of blanks, duplicates and standards, were maintained to obtain precise and accurate results.

3.b. LA-ICP-MS in situ zircon and monazite geochronology

In situ zircon and monazite U-Pb geochronology were performed on standard polished thin sections (thickness of 30 μm and 120 μm) at the University of New Brunswick. Analyses were performed using a Resonetics S-155-LR 193 nm ArF (excimer) laser ablation system coupled to an Agilent 8900 'triple quad' ICP-MS. The ablation work was supported by scanning electron microscope-backscattered electron imaging obtained at the UNB Microscopy and Microanalysis Facility with a JEOL LSM-6400 Scanning Electron Microscope using an accelerating voltage of 15 kV and 1 nA current. Images were acquired using a Digiscan II controlled by Gatan Digital Micrograph software. The monazite standards GSC8153, and 44 069 were used for calibration (GSC8153) and verifying accuracy of unknowns. All analyses comprised 30s of background analysis prior to 30s of sample ablation. The laser produced shallow (<3 μm) 8 μm diameter pits using 3 Hz pulse rate and laser fluence of 3 J/cm^2 . The zircon standards FC-1 and Plesovice were used for calibration and to check accuracy. The laser produced shallow 10–19 μm diameter pits using 3 Hz pulse rate and laser fluence of 3 J/cm^2 . Analyses were processed with Lolite v3.7.

3.c. Whole-rock Sm-Nd and Lu-Hf-isotope analysis

Four powdered samples of the dykes were prepared and measured in the Isotope Geochronology and Geochemistry Research Centre (IGGRC) at Carleton University. Rock powders were doped with a ^{148}Nd - ^{149}Sm mixed spike before they were dissolved in mixed concentrated HF and HNO_3 . The sample digests were also sequentially dissolved in 7M HNO_3 and in 6M HCl and were evaporated to dryness. Sample residues were then taken up in 2 ml 3M HCl and loaded onto prepacked 2 ml LN-resin columns (50 to 100 μm , Eichrom Technologies, LLC, USA). The columns were first washed with 15 ml 3M HCl and wash solutions were collected (containing other elements including Sr, light and middle rare elements (REEs)). The columns were then washed with 20 ml 6M HCl to remove Yb and Lu completely. Hf was finally eluted with 4 ml of 2M HF after Ti was eluted with 10 to 20 ml 4M HCl + 0.5% H_2O_2 .

Wash solutions from Hf columns were evaporated to dryness and the residues were dissolved in 1.5 ml of 2.5 M HCl and loaded onto 14-ml Bio-Rad borosilicate glass chromatography columns containing 3.0 ml of Bio-Rad AG50W-X8 cation exchange resin. Columns were washed with 16 ml of 2.5 M HCl before Sr was eluted with 7 ml of 2.5 M HCl. Columns were washed with 3.5 ml of 6M HCl before REEs were eluted using 9 ml of 6M HCl. REE fractions were dissolved in 0.26M HCl and loaded onto 2 ml

prepacked Ln resin columns (50 to 100 μm , Eichrom Technologies, LLC, USA). Nd was eluted using 0.26M HCl, followed by Sm elution using 0.5M HCl. Nd-isotope ratios were measured using IGGRC's Thermo-Finnigan Neptune MC-ICP-MS. Nd and Hf isotopic ratios were normalized against $^{146}\text{Nd}/^{144}\text{Nd} = 0.7219$ and $^{179}\text{Hf}/^{177}\text{Hf} = 0.7325$, respectively. $^{143}\text{Nd}/^{144}\text{Nd}$ ratios were also normalized to JNdi-1 average value 0.512100 measured by IGGRC's Thermo-Finnigan Triton TIMS.

The average values of reference materials for a period of five months covering this analysis session are NBS987 $^{87}\text{Sr}/^{86}\text{Sr} = 0.710240 \pm 0.000019$ (2SD, $n = 38$), JNdi-1 $^{143}\text{Nd}/^{144}\text{Nd} = 0.512095 \pm 0.000014$ (2SD, $n = 65$), JMC475 $^{176}\text{Hf}/^{177}\text{Hf} = 0.282164 \pm 0.000014$ ($n = 8$). In the last four years, the USGS rock standards' average values are BCR-2 $^{87}\text{Sr}/^{86}\text{Sr} = 0.705000 \pm 0.000027$ ($n = 37$), $^{143}\text{Nd}/^{144}\text{Nd} = 0.512625 \pm 0.000008$ ($n = 14$), $^{176}\text{Hf}/^{177}\text{Hf} = 0.282869 \pm 0.000016$ ($n = 5$); and BHVO-2 $^{87}\text{Sr}/^{86}\text{Sr} = 0.703485 \pm 0.00004$ ($n = 3$), $^{143}\text{Nd}/^{144}\text{Nd} = 0.512974 \pm 0.000011$ ($n = 6$), $^{176}\text{Hf}/^{177}\text{Hf} = 0.283113 \pm 0.000004$ ($n = 3$). The total procedure blanks were <50 pg for Nd and <70 pg for Hf. The Sm/Nd column procedures were also described in Cousens (1996) and Hf columns in Yang et al. (2010).

4. Results

4.a. Petrography of dykes

Leucocratic non-foliated dykes, with thickness varying between 10 cm and 50 cm, occur both parallel to and crosscut the foliation in the host rocks, i.e. the Millican Lake Granite and the Cape Spencer Formation, and exhibit a secondary earthy hematization that results in a pinkish red colouration (Figure 3(a)). The leucocratic dykes are exposed on the northern coast of the Bay of Fundy, around Cape Spencer and have also been identified inland in drill core. These low-angle (5–30°) sill-like bodies exhibit high variability in their attitude and vary from fine-grained to typically very fine-grained sugary aplites with sharp contacts (Figure 3(b) and c). Based on their mineral assemblage, these dykes are classified into albitites. Albite (50–90%) and quartz (5–40%) are the principal components of these dykes (Figure 3(d) and (e)); carbonate (1–5%) (Figure 3(f)) and K-feldspar (1–5%) constitute the second most important components. Accessory minerals include specularite, pyrite, zircon and monazite. The albite (An content less than 10%) is normally subhedral, with the development of twin lamellae and Carlsbad twins; chess-board albite also occurs (Figure 3(g)), characterized by a dense array of narrow discontinuous albite lamellae. These albites (0.1 to 0.5 mm) occur with clear and colourless rhomb carbonates (0.05 to 0.3 mm). X-ray diffraction patterns for the rhomb carbonate indicate that this is mostly ankerite. K-feldspar is a minor phase and is found as subhedral to anhedral plates, or as relics in albite in association with anhedral quartz crystals; the diameters of the quartz and K-feldspar crystals vary from 0.02 to 0.5 mm. Both albite and quartz host small inclusions of carbonate.

4.b. Major- and trace-elements characteristics

Chemical discrimination by means of the multi-cationic diagram from De la Roche et al. (1980) results in samples forming a continuous spectrum from nepheline syenite to granite fields (Figure 4(a)), despite the samples having few K-feldspar and evident low K_2O contents, reflecting the ultrasodic composition of

these dykes. All samples are metaluminous ($\text{A}/\text{CNK} = 0.74\text{--}0.96$), except for AP-08 ($\text{A}/\text{CNK} = 1.10$) (Figure 4(b)).

Major element concentration data for the dykes are provided in Table 1. The felsic dykes have a wide range of chemical compositions, with $\text{SiO}_2 = 58.94\text{--}79.24$ wt.%, $\text{Al}_2\text{O}_3 = 10.50\text{--}18.50$ wt.%, $\text{Na}_2\text{O} = 5.50\text{--}10.89$ wt.% and $\text{CaO} = 0.38\text{--}3.88$ wt.%. In general, most major oxides are negatively correlated with SiO_2 , except for K_2O and TiO_2 (Figure 5).

The trace-element compositions for the Cape Spencer dykes are provided in Table 2. Primitive-mantle normalized (Sun & McDonough, 1989) spider diagrams (Figure 6(a)) show enrichment in Th and U and depletion in high field strength elements (HFSEs: Nb, P, and Ti). Taken collectively, the abundances of large-ion lithophile elements (LILEs: Cs, Rb, Ba, and Sr) are low relative to the average crustal values from Taylor & McLennan (1995) [$\text{Cs} (\leq 0.4$ ppm), $\text{Rb} (\leq 21$ ppm), $\text{Ba} (\leq 185$ ppm), and $\text{Sr} (\leq 172$ ppm)]. Chondrite-normalized REE patterns show similar negatively sloping rare earth elements, moderately to slight light rare element enrichment ($\text{La}_\text{N}/\text{Sm}_\text{N} = 4.8\text{--}18.7$), slightly positive heavy REE slopes ($\text{Gd}_\text{N}/\text{Yb}_\text{N} = 0.4\text{--}1.4$) and variable ($\text{La}_\text{N}/\text{Yb}_\text{N}$) ratios [REE, ($\text{La}/\text{Yb})_\text{N} = 3.02\text{--}39.62$, where N indicates chondrite normalized with values from Sun & McDonough (1989)]. Europium anomalies are slightly negative for all aplitic samples [$(\text{Eu}_\text{N}/\text{Eu}^*) = 0.72\text{--}0.95$, where $\text{Eu}^* = \sqrt{(\text{Sm}_\text{N} \times \text{Gd}_\text{N})}$] (Figure 6(b); Table 1).

The Nb/Ta ratios (Figure 7(a)) are much lower than primitive mantle and mantle-derived melts, including both mid-ocean ridge basalts and ocean island basalts (avg. $\text{Nb}/\text{Ta} = 17.5 \pm 2$; Green, 1995) and the Earth's mantle ($\text{Nb}/\text{Ta} \sim 16$; Pfänder et al. 2007; Arevalo & McDonough, 2010); the ratios are also lower than in the average continental crust, i.e. $\text{Nb}/\text{Ta} \sim 11$ (Taylor & McLennan, 1985, 1995; Green, 1995; Rudnick & Gao, 2014). Some of the samples plot below $\text{Nb}/\text{Ta} \sim 5$, a ratio suggested to represent a threshold between purely magmatic systems ($\text{Nb}/\text{Ta} > 5$) and magmatic-hydrothermal systems ($\text{Nb}/\text{Ta} < 5$) (Ballouard et al. 2016). Zr/Hf ratios are lower than the range 33–40, which includes values of both chondrites and crust defined by Jochum et al. (1986). Magmatic affinity was also determined using the parameters of Ross & Bédard (2009) (Figure 7(b)); dykes plot in the calc-alkaline magmatic affinity field, an indication of mixing of different magma sources consistent with subduction zone magmas where the breakdown of hydrous minerals occurs resulting in the liberation of aqueous solutions (Kelley & Cottrell, 2009; Zheng, 2019; Vermeesch & Pease, 2021).

On tectonomagmatic discrimination diagrams (Whalen & Hildebrand, 2019), the dykes fall within the slab failure field of the Nb vs. Y and Ta vs. Yb diagrams (Figure 8(a) and (b)). In the Rb vs. Y + Nb and Rb vs. Ta + Yb diagrams (not shown), most samples plot in the arc field; however, there are some samples plotting in the slab failure field or close to the boundary, resulting from the relative mobility of Rb. However, when using the fields from Pearce et al. (1984), samples plot in the volcanic-arc granite (VAG) field, except in the case of the Ta vs. Yb where there is spread of data from the VAG field into the syn-collision granite field, probably reflecting fractionation and crustal contamination, as this classification scheme tends to reflect magmatic sources rather than tectonic setting (Pearce, 1996; Förster et al. 1997). The use of other discriminators (Hildebrand & Whalen, 2014) (not shown), such as Sr/Y, La/Yb and Sm/Yb, results in samples plotting in both fields, whereas Gd/Yb results in all samples plotting in the arc field.

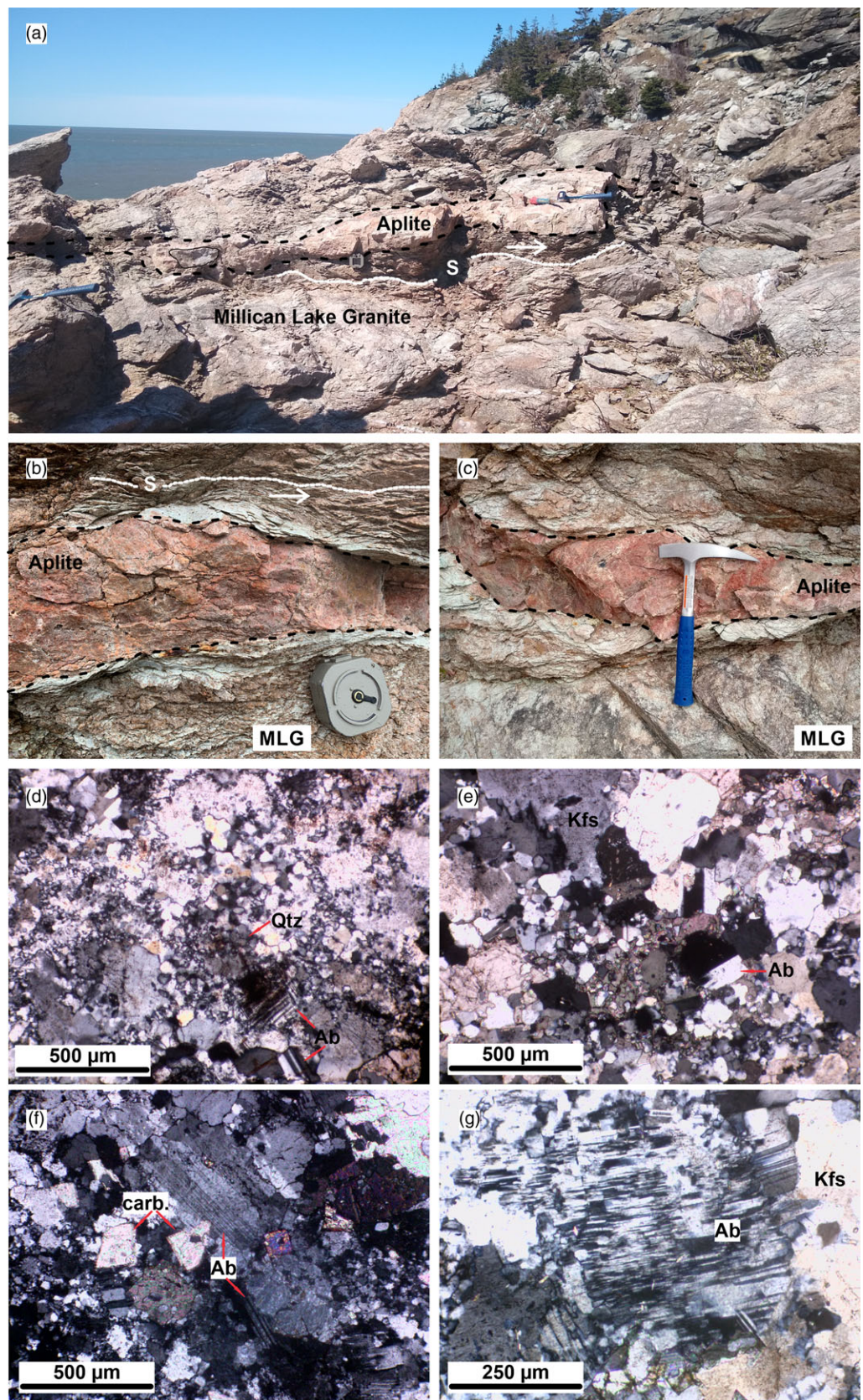


Figure 3. (Colour online) Field photographs and polished thin section photomicrographs of the aplitic textured leucogranitic dykes in the Cape Spencer area. (a) Aplitic dyke intruding the Millican Lake Granite following its foliation (S). (b) Aplitic dyke exhibiting its characteristic pinkish-red colouration in sharp contact with the host rock. (c) Specularite in aplitic dyke. (d) Tonalitic dyke (XPL). (e) Albitite dyke (XPL). (f) Carbonates with albite. (g) Chess-board albite. Qtz: quartz, Carb.: carbonate, Ab: albite, Kfs: K-feldspar.

All the samples have an alumina saturation index of less than 1.1 and SiO_2 concentration between 58.9 and 79.24 wt.%, exceeding the limit of 70 wt.% under which these discrimination diagrams

are valid (Hildebrand & Whalen, 2017); however, there is no correlation in samples with high SiO_2 being plotted on a specific field.

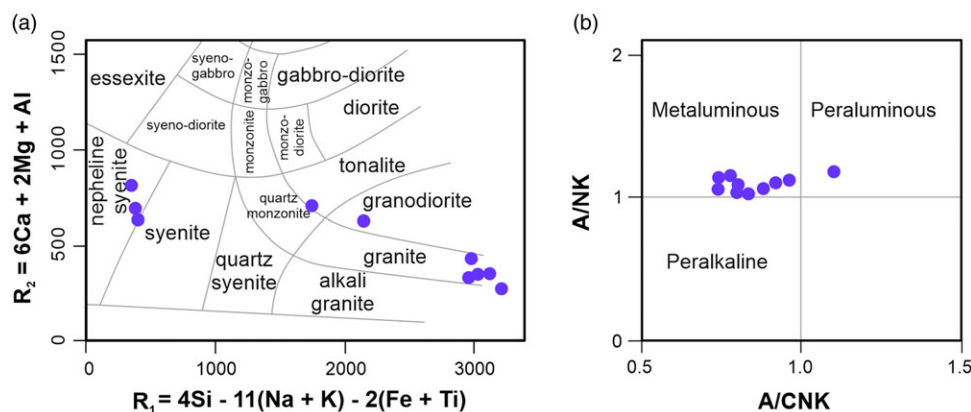


Figure 4. (Colour online) (a) R_1 - R_2 multi-cationic classification diagram (De la Roche *et al.* 1980). (b) Chemical composition – Shand index plot. Fields are from Maniar and Piccoli (1989); $A/CNK = Al_2O_3 / (CaO + Na_2O + K_2O)$, $A/NK = Al_2O_3 / (Na_2O + K_2O)$, in moles.

4.c. Geochronology

Regardless of the attempts to avoid ablating fractures or inclusions while at the same time targeting specific domains so the effects of mixing could be controlled, samples display a dispersion of U-Pb data related to recent Pb-loss, common-Pb incorporation and inheritance. Zircons in these aplite samples are, for the most part, anhedral very fine grains up to 45–50 μm in size; these grains exhibit radiation damage (Figure 9(a)–(c)), elevated U (2000 – 94 000 ppm) and Th (500 – 45 000 ppm) concentrations, extensive microfracturing and to a large extent lack oscillatory zoning. Monazite within the dykes occurs as subhedral to anhedral very fine grains up to 25–30 μm in size that locally exhibit faint patchy zoning that resembles an outermost domain and a core (Figure 9(d)–(f)).

Zircon grains were analyzed (Supplementary Table S1) with the resulting data exhibiting significant common-Pb contamination necessitating correction to all ablated spots (common-Pb corrected using the measured ^{204}Pb). Despite the correction, most spots are usually discordant (Figure 10(a)), which indicates a small residual ^{204}Pb component below the instrument's detection limit. The relative probability plot suggests most of the spots correspond to inherited material dating back to ca. 650 Ma (Figure 10(b)). There are two young populations, a small cluster around 275 Ma and an older group around 350 Ma, when plotting the data on a Wetherill Concordia diagram. Considering both the high degree of metamictization in zircon and textural setting that prevents the identification of rims, cores or zoning, the best estimate for the zircon crystallization age is based on a weighted mean $^{206}Pb/^{238}U$ age of 273.4 ± 4.2 Ma (MSWD = 1.03; $n = 4$), for the youngest cluster (Figure 10(d)), whereas the older group is 348.5 ± 3.1 Ma (MSWD = 0.53; $n = 5$), also based on a weighted mean $^{206}Pb/^{238}U$ age (Figure 10(c)).

Monazite grains were analyzed using an 8 μm crater size (Supplementary Table S2), considering the small size of most grains; it was not possible to measure ^{204}Pb , although it is present considering the Pb/U ratios. The results show a spread of data interpreted as the mixing between two different age domains. Assuming all samples are cogenetic and using $^{207}Pb/^{206}Pb$ based on a terrestrial model, it is possible to perform an anchored ($^{207}Pb/^{206}Pb = 0.85 \pm 0.01$) Tera-Wasserburg regression, an age of 273.7 ± 1.3 Ma (MSWD = 0.29; $n = 3$) corresponding to the youngest end-member age population is determined (Figure 11(a)). A lower intercept age of 273.2 ± 9.2 (MSWD = 2.2) is obtained when plotting the monazite data on a conventional Concordia diagram (Figure 11(b)).

4.d. Whole-rock Hf-Nd isotopes

The ($^{176}Hf/^{177}Hf$)_i ratios in the Cape Spencer dykes samples range from 0.282561 to 0.282585, based on an age of 274 Ma, with ϵHf values in the range from -1.8 to -1.0, calculated at the same age (Table 3). The initial ($^{143}Nd/^{144}Nd$)_i ratios observed in four samples from this study range from 0.511785 to 0.511993, based on an age of 274 Ma, with ϵNd values in the range from -9.7 to -5.7, calculated at the same age, and TDM values of 1.3–1.6 Ga (Table 3).

5. Discussion

5.a. Petrogenesis

The Cape Spencer dykes can be classified as albitites, based on their modal mineralogy, with high Na_2O (av. 7.36) and low K_2O/Na_2O (av. 0.04), average molar A/CNK of 0.85 and A/NK of 1.11 (Figure 4(b)). Their metaluminous affinity, zircon content (24–101 ppm) and decreasing P_2O_5 with increasing SiO_2 are characteristics of low-temperature I-type granitoids (Chappell & White, 2001; Chappell *et al.* 2004). The lack of parallel fabrics and the presence of replacement textures in the dykes indicate that the albitization process, in which K-feldspar was consumed, was of internal origin, i.e. autometasomatism, rather than metamorphism as the host rocks show no indication of alteration by a later event. There is a large range in loss on ignition, up to almost 5 wt.%, and it directly correlates with CaO, which indicates the suppression of An-content and crystallization of primary carbonate minerals (cf. Holloway, 1976). The primary nature of the (rhomb) carbonates is supported by the presence of inclusions in quartz and albite and the occurrence of single crystals. Although considered rare, the presence and crystallization of carbonates from granitic melts are constrained to pressures above 3 kbar (Swanson, 1979; Audéat *et al.* 2004).

These dykes also reflect depletion in Nb, P and Ti, but enrichment in Cs, U and Th, which are typical features of magmas originating in a subduction zone (Taylor & McLennan, 1985; Hofmann, 1988; Bea *et al.* 2011). In general, the Caledonia terrane plutons (ca. 630–615 Ma) associated with the Broad River Group share most of these characteristics (Whalen *et al.* 1994; Barr & White, 1996b). Slab failure-related rocks derived through deep mantle processes that, for the most part, include partial melting of the upper portion of the torn slab (Hildebrand & Whalen, 2014, 2017; Whalen & Hildebrand, 2019); the use of immobile element geochemical discriminators (Whalen & Hildebrand, 2019) resulted in data plotting in both the slab failure and arc-related fields.

Table 1. Major element concentrations (wt.%) for the dykes studied. LOI = loss on ignition

Sample	AP-01	AP-02	AP-03	AP-04	AP-07	AP-08	AP-09	AP-10	AP-11	AP-12
SiO ₂	58.94	79.24	77.52	61.94	66.29	79.20	68.89	78.11	76.38	64.79
Al ₂ O ₃	17.31	10.95	10.52	17.66	13.73	11.20	12.82	11.38	10.50	18.50
Fe ₂ O ₃ ^T	2.23	0.74	1.10	2.00	2.55	0.76	1.62	1.10	1.34	1.21
MnO	0.111	0.032	0.024	0.081	0.086	0.020	0.091	0.022	0.055	0.070
MgO	0.99	0.24	0.16	0.85	1.07	0.11	0.97	0.19	0.31	0.35
CaO	3.88	1.10	1.19	2.78	3.52	0.38	2.99	0.85	1.90	2.31
Na ₂ O	9.87	5.66	5.82	10.35	7.10	5.50	6.45	6.14	5.83	10.89
K ₂ O	0.05	0.55	0.17	0.06	0.34	0.40	0.43	0.15	0.03	0.04
TiO ₂	0.082	0.095	0.157	0.107	0.135	0.085	0.286	0.111	0.077	0.072
P ₂ O ₅	0.07	0.04	0.02	0.09	0.04	0.02	0.06	< 0.01	0.02	0.06
LOI	4.95	1.98	1.77	4.26	5.02	0.82	4.23	1.22	2.26	2.61
Total	98.5	100.6	98.5	100.2	99.9	98.5	98.9	99.3	98.7	100.9
A/CNK	0.74	0.92	0.88	0.80	0.74	1.10	0.77	0.96	0.80	0.83

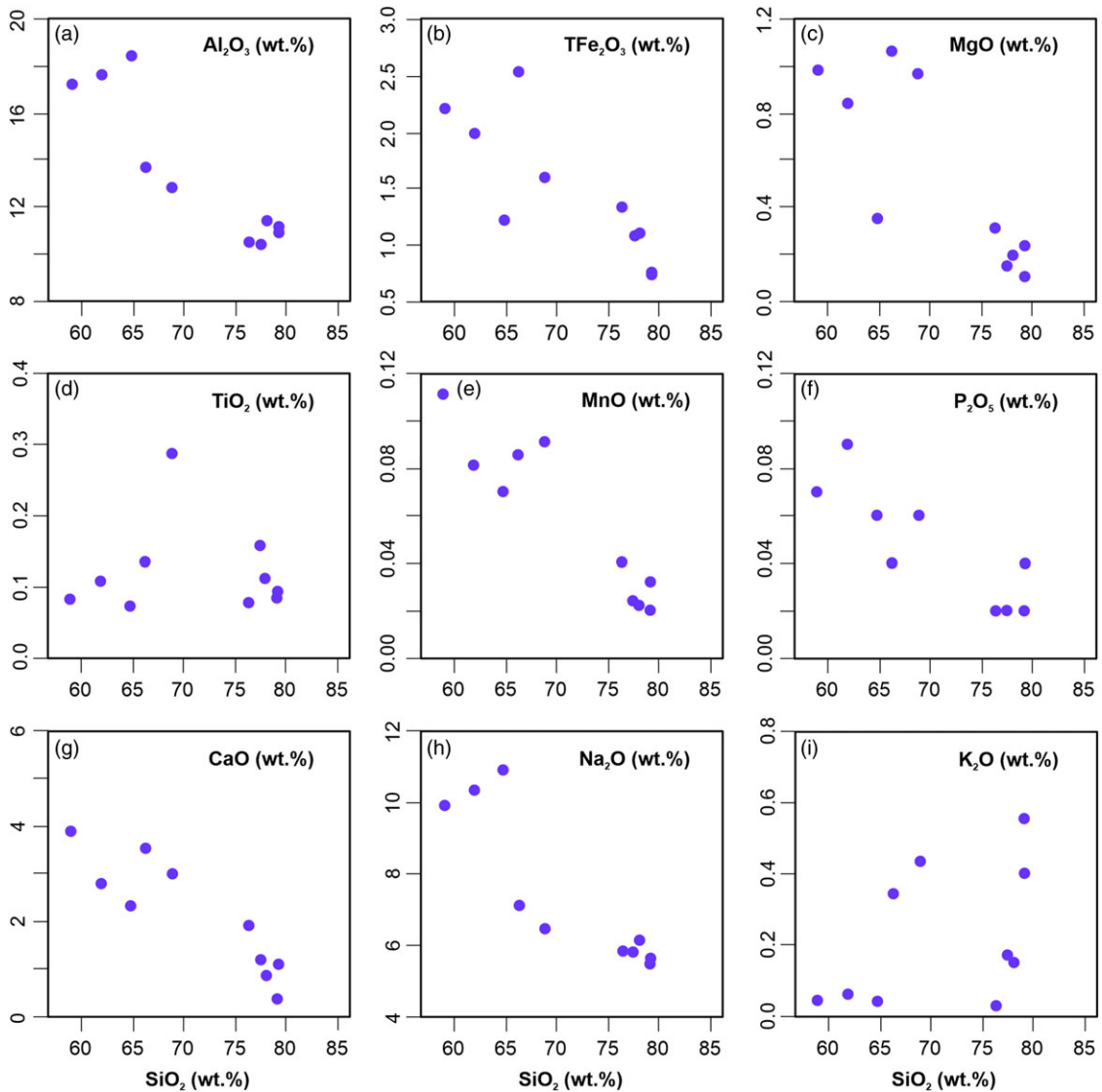
**Figure 5.** (Colour online) Representative Harker diagrams for the dykes showing variations of selected elements (versus SiO₂).

Table 2. Trace elements compositions (ppm) for the dykes studied

Sample	AP-01	AP-02	AP-03	AP-04	AP-07	AP-08	AP-09	AP-10	AP-11	AP-12
Sc	3	1	<1	2	3	<1	4	<1	1	2
Be	<1	<1	<1	<1	<1	<1	<1	<1	<1	<1
V	<5	11	10	5	14	9	18	7	8	<5
Cr	<20	30	20	<20	<20	<20	<20	<20	<20	<20
Co	1	1	1	2	4	1	3	1	1	<1
Ni	<20	<20	<20	<20	<20	<20	<20	<20	<20	<20
Cu	<10	<10	<10	<10	20	840	110	<10	<10	30
Zn	30	<30	<30	30	40	<30	<30	<30	<30	<30
Ga	10	8	7	10	8	7	8	8	8	9
Ge	1.2	1.1	0.5	1.2	1	0.8	1	1	0.9	1.1
As	<5	<5	<5	<5	<5	14	7	5	<5	<5
Rb	1	21	6	2	14	17	18	6	1	1
Sr	166	58	100	172	185	71	89	91	69	156
Y	7.3	6.8	8.0	4.6	6.6	2.4	5.4	7.8	4.5	4.7
Zr	24	42	80	31	64	33	101	90	37	40
Nb	13.1	8.6	10.9	7.5	2.4	2.0	3.2	10.4	2.6	2.5
Mo	<2	3	2	<2	2	<2	<2	2	<2	<2
Ag	<0.5	<0.5	<0.5	<0.5	<0.5	<0.5	<0.5	<0.5	<0.5	<0.5
In	<0.1	<0.1	<0.1	<0.1	<0.1	<0.1	<0.1	<0.1	<0.1	<0.1
Sn	<1	<1	<1	<1	<1	<1	<1	2	<1	<1
Sb	0.4	0.6	0.3	0.4	1.3	5.3	3.8	0.6	0.4	0.3
Cs	<0.1	0.4	0.2	<0.1	0.2	0.3	0.3	0.3	0.1	<0.1
Ba	52	89	80	57	113	185	82	61	33	47
La	24.8	11.9	10.2	35.9	21.2	13.6	17.2	6.7	3.7	15.5
Ce	39.7	21.6	18.8	43.2	33.1	19.7	33.0	11.7	5.8	23.2
Pr	3.78	2.12	1.74	3.2	3.0	1.56	3.51	1.06	0.58	1.98
Nd	11.7	6.89	5.67	9.14	9.42	4.62	11.8	3.59	2.11	5.78
Sm	1.82	1.02	0.98	1.24	1.62	0.63	2.02	0.77	0.50	0.97
Eu	0.446	0.244	0.276	0.299	0.411	0.166	0.406	0.209	0.137	0.217
Gd	1.35	0.83	0.93	0.94	1.29	0.45	1.33	0.79	0.54	0.88
Tb	0.22	0.16	0.15	0.15	0.19	0.07	0.20	0.16	0.11	0.15
Dy	1.32	1.03	0.90	0.87	1.22	0.40	1.09	1.06	0.74	0.9
Ho	0.25	0.22	0.20	0.16	0.25	0.08	0.21	0.23	0.16	0.17
Er	0.74	0.67	0.78	0.49	0.76	0.26	0.64	0.83	0.49	0.48
Tm	0.111	0.11	0.155	0.084	0.123	0.052	0.093	0.161	0.084	0.079
Yb	0.77	0.78	1.48	0.65	0.95	0.43	0.70	1.59	0.63	0.6
Lu	0.128	0.137	0.313	0.119	0.187	0.082	0.133	0.289	0.123	0.116
Hf	1.0	1.4	3.2	1.4	2.6	1.6	2.7	4.8	1.8	1.8
Ta	1.29	0.99	1.32	4.24	0.48	0.40	0.42	1.79	0.58	0.28
W	2.9	<0.5	<0.5	3.0	1.7	1.0	3.7	3.8	2.2	1.5
Tl	0.05	0.29	<0.05	0.09	0.09	<0.05	<0.05	0.05	<0.05	<0.05
Pb	5	<5	6	<5	6	<5	<5	<5	<5	<5
Bi	<0.1	<0.1	<0.1	<0.1	<0.1	0.3	<0.1	0.1	<0.1	0.1

(Continued)

Table 2. (Continued)

Sample	AP-01	AP-02	AP-03	AP-04	AP-07	AP-08	AP-09	AP-10	AP-11	AP-12
Th	38.5	35.4	59.5	44.0	31.1	26.8	15.1	47.3	31.5	29.1
U	3.80	3.20	8.02	3.49	3.38	2.74	1.89	6.67	3.54	3.35
Th/U	10.13	11.06	7.42	12.61	9.20	9.78	7.99	7.09	8.90	8.69
Eu _N /Eu*	0.87	0.81	0.88	0.85	0.87	0.95	0.76	0.82	0.81	0.72
La _N /Yb _N	23.10	10.94	4.94	39.62	16.01	22.69	17.63	3.02	4.21	18.53
La _N /Sm _N	8.80	7.53	6.72	18.69	8.45	13.94	5.50	5.61	4.78	10.32
Gd _N /Yb _N	1.45	0.88	0.52	1.20	1.12	0.87	1.57	0.41	0.71	1.21
Sr/Y	22.7	8.5	12.5	37.4	28.0	29.6	16.5	11.7	15.3	33.2
La/Yb	32.2	15.3	6.9	55.2	22.3	31.6	24.6	4.2	5.9	25.8
Gd/Yb	1.8	1.1	0.6	1.4	1.4	1.0	1.9	0.5	0.9	1.5
Sm/Yb	2.4	1.3	0.7	1.9	1.7	1.5	2.9	0.5	0.8	1.6
INAA										
Au (ppb)	< 2	< 2	< 2	< 2	< 2	30	252	< 2	< 2	< 2
As	1.5	3.5	2.8	1.7	3.9	18.2	6.7	4.3	5.1	2.2
Br	< 0.5	< 0.5	< 0.5	< 0.5	< 0.5	< 0.5	< 0.5	< 0.5	< 0.5	< 0.5
Cr	< 5	25	21	< 5	< 5	< 5	< 5	< 5	< 5	< 5
Ir (ppb)	< 5	< 5	< 5	< 5	< 5	< 5	< 5	< 5	< 5	< 5
Sc	2.9	0.7	0.7	2.0	2.5	0.8	3.4	0.6	1.2	2
Se	< 3	< 3	< 3	< 3	< 3	< 3	< 3	< 3	< 3	< 3
Sb	0.4	0.8	0.4	0.5	1.4	6.0	4.5	0.6	0.8	0.6

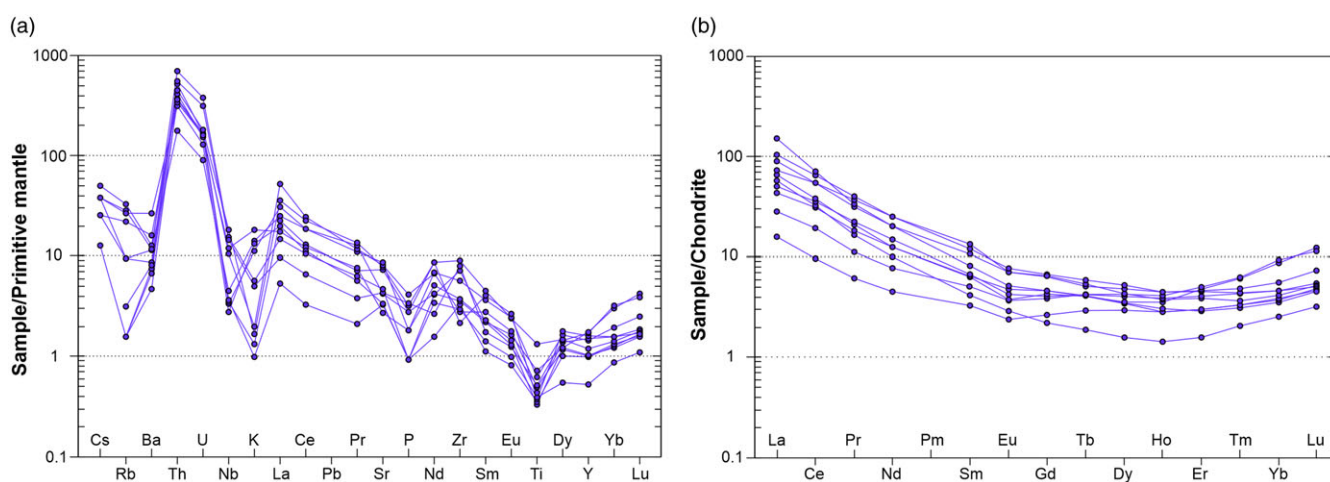


Figure 6. (Colour online) (a) Primitive-mantle normalized trace-element diagram. (b) Chondrite-normalized rare earth element diagram. Normalization factor after Sun & McDonough (1989).

Overall, the low Nb/Ta ratios of these dykes constitute an intracrustal differentiation feature (Tang *et al.* 2019; Ballouard *et al.* 2020) and the low Zr/Hf ratios are characteristic of highly evolved magmatic rocks that have been derived through selective partial melting, then through fractional crystallization combined with hydrothermal interaction with released magmatic fluids (autometasomatic) (Bau, 1996; Tartèse & Boulvais, 2010). The Th and U averages in the Cape Spencer dykes are 35.8 ppm and 4.0 ppm, respectively. The Th/U ratios vary from 7.42 to 12.61,

higher than the Th/U ~ 4 accepted for both the crustal and mantle domains (Artemieva *et al.* 2017; Wipperfurth *et al.* 2018), although it is known that Th/U ratios vary greatly in felsic rocks between 1 and 10 (Hasterok *et al.* 2018), and that for some I-type granitoids, both Th and U contents increase with differentiation (Champion & Chappell, 1992; Villaseca *et al.* 1998). These high Th/U ratios had to be, for the most part, inherited from the source and probably further enhanced by fractional crystallization and/or magma mixing (Scharfenberg *et al.* 2019). The slightly negative

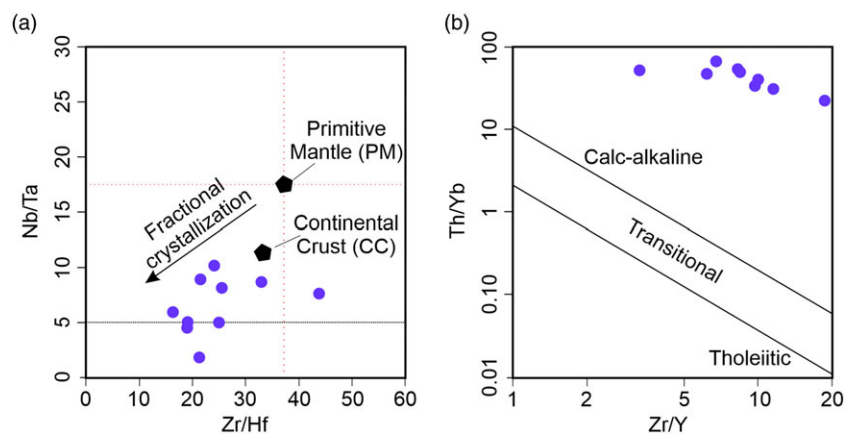


Figure 7. (Colour online) Trace element-based discrimination diagrams. (a) Nb/Ta vs. Zr/Hf diagram. Primitive mantle data are from McDonough & Sun (1995) and continental crust data are from Taylor & McLennan (1985). (b) Th/Yb vs. Zr/Y diagram for discrimination of magmatic affinities. Modified from Ross & Bédard (2009).

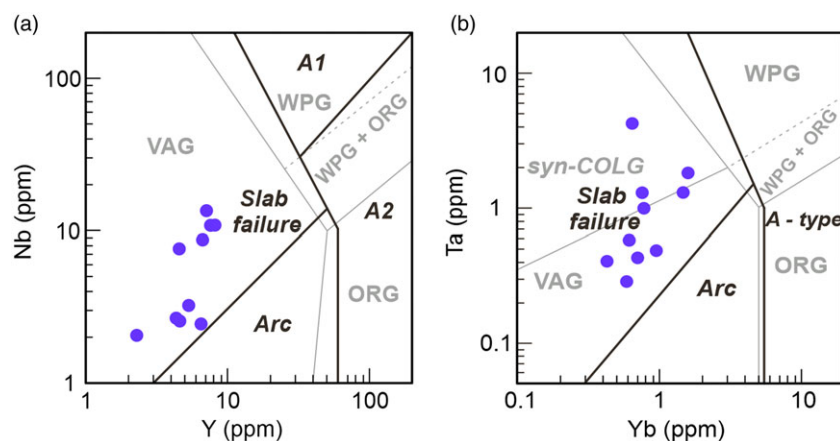


Figure 8. (Colour online) Tectonomagmatic discrimination diagrams for dykes samples from the Cape Spencer area (Whalen & Hildebrand, 2019). (a) Nb vs. Y. (b) Ta vs. Yb. Fields in grey are from Pearce *et al.* (1984).

Eu-anomalies ($Eu_N/Eu^* = 0.72\text{--}0.95$) may indicate early fractionation of primary plagioclase associated with a reduced melt.

5.b. Estimation of liquidus temperature

Temperatures of the magmas of these dykes are estimated using zircon, monazite and apatite solubility models. Considering the major element concentrations, the low Zr concentrations in the dykes yielded zircon saturation temperatures ($T_{ZircSat}$) of approximately 590–738 °C (average = 670 °C) [calculations using the formula of Watson & Harrison (1983)]. It must be stated that $T_{ZircSat}$ was calibrated for rocks with whole-rock compositions ranging from $M = 0.9\text{--}1.9$ (Watson & Harrison, 1983). This M value [$M = (Na + K + 2Ca)/(Al.Si)$] is a compositional parameter calculated by obtaining the molar amounts of each component, renormalizing and finally obtaining the ratio (Boehnke *et al.* 2013); M is essentially controlled by the silica content of the melt (Siégel *et al.* 2018), i.e., the lower the silica content of the melt the higher the value of the M parameter, resulting in decreasing $T_{ZircSat}$ for granitic magmas that are produced by fractional crystallization of mafic magmas (Harrison *et al.* 2007). AP-01, AP-04, AP-07, AP-09 and AP-12 have M values of 1.9–2.4. The textural consistency of these dykes suggests rapid crystallization from a residual melt, with the consequent quenching in response to a rapid pressure drop. The dykes from Cape Spencer can be considered inheritance-rich intrusions. Although they constitute late segregated melts, the $T_{ZircSat}$ should indicate an upper limit on the magma temperature

and, therefore, a useful estimate of the initial magma temperature at the source (Miller *et al.* 2003). The average $T_{ZircSat}$ and the low concentrations of zirconium reinforce the classification of these dykes as true low-temperature melts (Brown, 2013), as there is no indication of sequestration of zircon (Bea, 1996). Monazite-saturation geothermometry (Montel, 1993), using the bulk REE composition ($\sum REE_i = La + Ce + Pr + Nd + Sm + Gd$) to represent the melt composition and assuming 3 wt.% H_2O content yields temperatures ($T_{Monazite}$) of 562–690 °C. Some of the $T_{Monazite}$ values are higher than $T_{ZircSat}$ values, suggesting the presence of additional REE-bearing phases.

5.c. Emplacement age and relation to gold mineralization

The dykes have an age of 273.7 ± 1.3 Ma based on U-Pb dating of monazite and constitute the youngest Alleghanian magmatic event in southern New Brunswick to this date. Because of the metamict nature of the zircon grains, an independent constraint was necessary to evaluate the meaning of the altered zircon ages. In this study, coexisting monazite geochronology supports the ~274 Ma age from the altered zircons as the crystallization age. This age is also younger than the Ar-Ar ages (276.6 ± 0.9 and 283.7 ± 0.8 Ma) obtained by Watters (1993) on illites defining the fabrics associated with gold mineralization. Most aplitic dyke samples analyzed in this study contain low Au (<2 ppb), As (≤ 5.1 ppm), and Sb (≤ 1.8 ppm). Only samples AP-08 and AP-09 contain values above the detection limit for Au: 30 ppb and 252 ppb, respectively, and

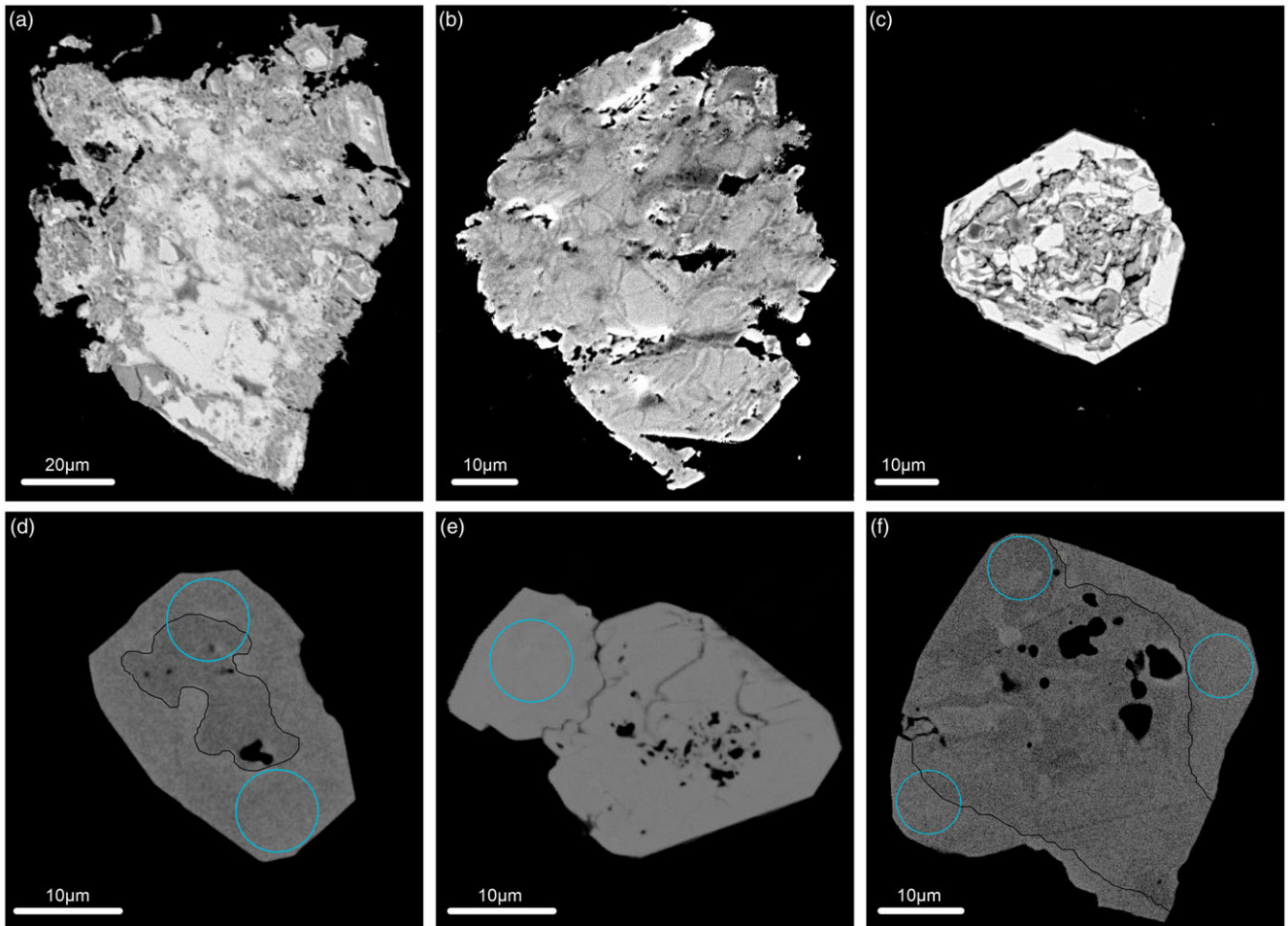


Figure 9. (Colour online) Scanning electron microscope-backscattered electron imaging of zircons (a–c) and monazites (d–f). (a–c) Metamictic zircons showing massive radiation damage. (d) Subhedral monazite displaying patching zoning (dotted black line). (e) fractured homogeneous subhedral monazite. (f) Subhedral rounded monazite displaying patchy zoning (dotted black line). Light blue circles correspond to spot locations (8 μm for monazite).

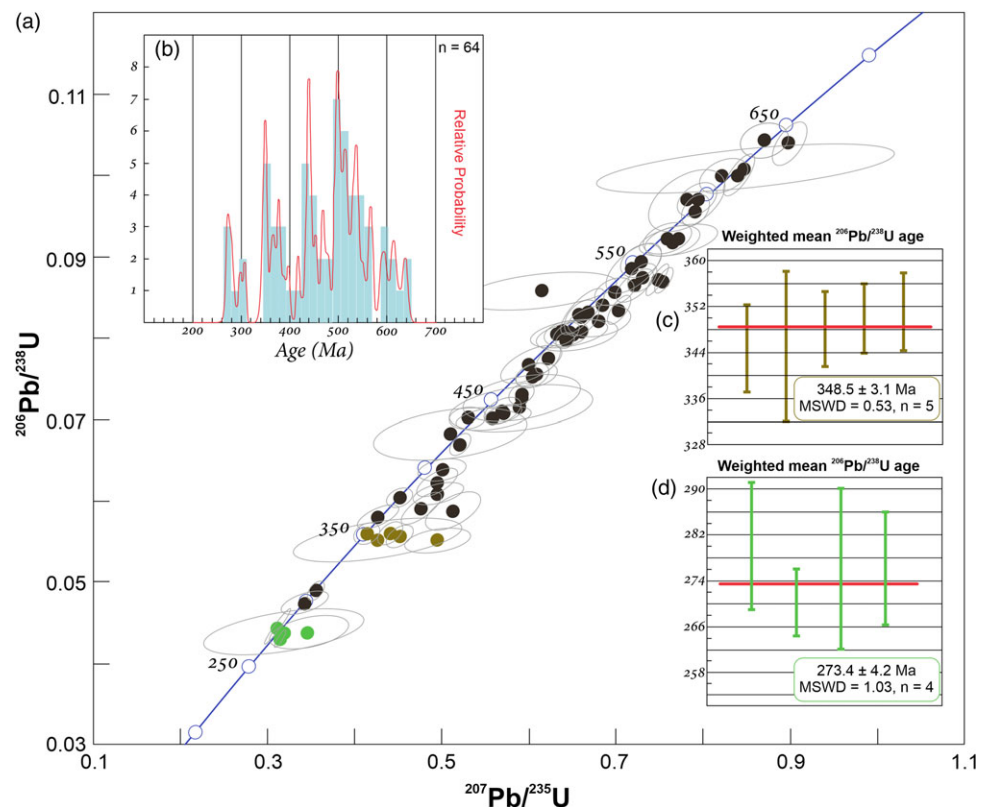


Figure 10. (Colour online) LA-ICP-MS results of U–Pb zircon geochronology of samples from Cape Spencer. (a) Wetherill Concordia diagram for all data. (b) Relative probability plot and age histograms for zircon U–Pb ages. Bin width is approximately 20 Ma. (c) Weighted mean plot of $^{206}\text{Pb}/^{238}\text{U}$ ages for the older population. (d) Weighted mean plot of $^{206}\text{Pb}/^{238}\text{U}$ ages for the youngest population. Error bars are 2σ .

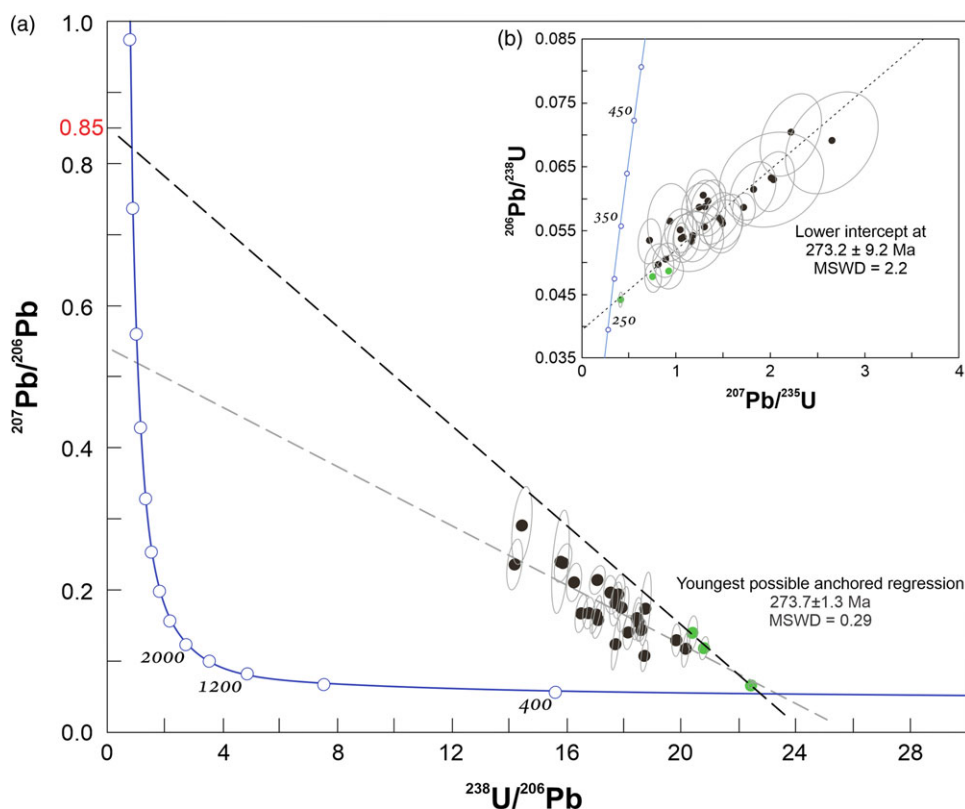


Figure 11. (Colour online) LA-ICP-MS results of U-Pb monazite geochronology of aplitic samples from Cape Spencer. (a) Tera-Wasserburg Concordia diagram for all data. The grey dashed line indicates a free regression through the data resulting in a nonviable low common $^{207}\text{Pb}/^{206}\text{Pb}$ intercept. (b) Conventional Concordia diagram for all data indicating a not anchored lower intercept at 273.2 ± 9.2 Ma.

Table 3. Nd and Hf isotopic data for the dykes from Cape Spencer

Sample	Nd (ppm)	Sm (ppm)	$^{143}\text{Nd}/^{144}\text{Nd}_m$	2σ	$(^{143}\text{Nd}/^{144}\text{Nd})_i$	ϵNd	T_{DM} (Ma)
AP-01	8.380	1.352	0.511991	± 10	0.511816	-9.2	1515
AP-02	7.277	1.139	0.512075	± 10	0.511905	-7.4	1371
AP-03	5.894	1.005	0.511970	± 10	0.511785	-9.8	1618
AP-04	4.658	0.804	0.512180	± 10	0.511993	-5.7	1346
Sample	Lu (ppm)	Hf (ppm)	$^{176}\text{Hf}/^{177}\text{Hf}_m$	2σ	$(^{176}\text{Hf}/^{177}\text{Hf})_i$	ϵHf	
AP-01	0.128	1.00	0.282677	± 6	0.282583	-1.0	
AP-02	0.137	1.40	0.282632	± 4	0.282561	-1.8	
AP-03	0.313	3.20	0.282644	± 4	0.282573	-1.4	
AP-04	0.119	1.40	0.282646	± 6	0.282585	-1.0	

Note: Age correction for $(^{143}\text{Nd}/^{144}\text{Nd})_i$, $(^{176}\text{Hf}/^{177}\text{Hf})_i$, ϵNd , and ϵHf is 274 Ma. T_{DM} was calculated using a linear evolution for a mantle separated from the chondritic uniform reservoir at 4.55 Ga with a present-day epsilon value of +10.

contain higher amounts of As (18.2 ppm and 6.7 ppm) and Sb (6.0 ppm and 4.5 ppm). Furthermore, low values of Ag (<0.5 ppm), Cu (<10 ppm), Pb (≤ 8 ppm), Sn (<2 ppm), W (≤ 3.8 ppm) and Mo (≤ 3 ppm) are consistent with the idea that there is no genetic link between the dykes and the gold mineralizing event in the Cape Spencer area.

It can be argued that the two clusters of zircon ages represent: 1) a phase of sodic metasomatism along the MFZ resulting in highly albitized granites and albite+quartz veins (the aplites of this study) around 350 Ma; 2) later fluid flow related to young hydrothermal zircon and monazite around 275 Ma. Examples of the former option are the intrusion (ca. 362–350 Ma) of granites and related dykes into the Tournaisian Horton Group (Dunning *et al.* 2002; Koukouvelas *et al.* 2002; Malay *et al.* 2023), and sodic alteration in the Cobequid Shear Zone dated by riebeckite ($\sim 355 \pm 4$ Ma)

(Pe-Piper *et al.* 2018). Regarding the younger cluster, several indications could be used to interpret the 275 Ma cluster as having recorded a hydrothermal event in the region. Firstly, ^{40}Ar - ^{39}Ar ages (~ 327 Ma) reflect fluid flow coeval with dextral shear along the Avalonia-Meguma boundary (Murphy & Collins, 2008). Secondly, hydrothermal veins containing allanite and pyrite (~ 320 – 310 Ma) cut the Horton Group (Pe-Piper *et al.* 2018). Thirdly, hydrothermal mineralization associated with Zr-F-rich fluid complexes produced two zircon populations at ~ 318 Ma and ~ 309 Ma at Debert Lake, Nova Scotia (Ersay *et al.*, 2022), in the context of the presence of fluorine to transport Zr (Rb-Sr on illite: 300 ± 6 Ma, associated to Pb-Zn and barite mineralization) in the Cobequid Shear Zone, Nova Scotia (Pe-Piper & Piper, 2021; Ravenhurst *et al.* 1989). Nonetheless, the already established magmatic origin of these dykes rules out the possibility of the obtained age to represent

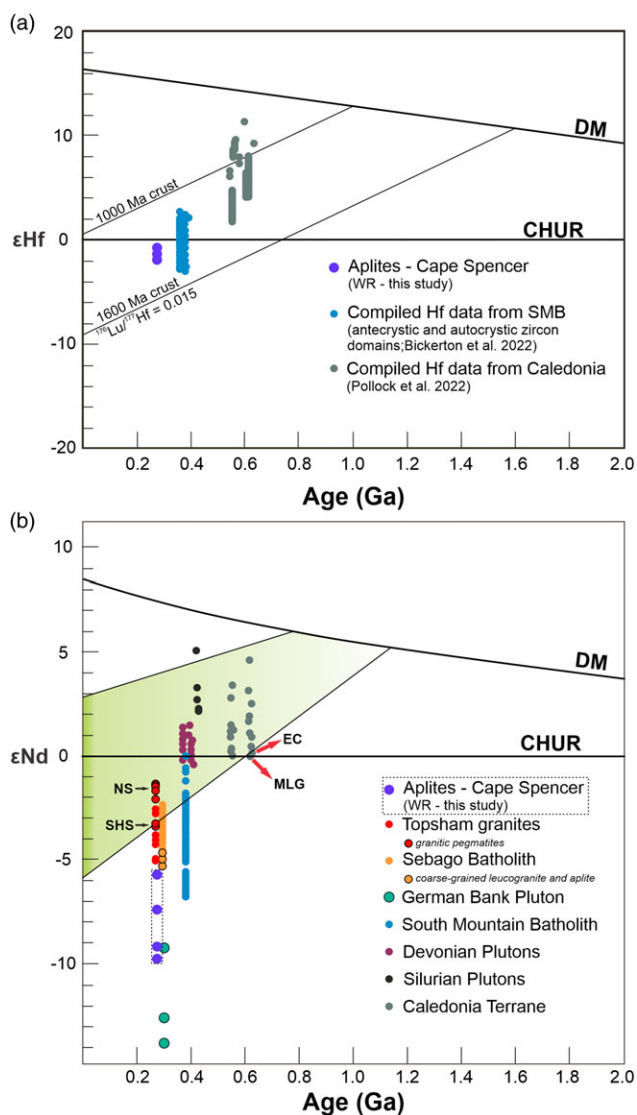


Figure 12. (Colour online) (a) Hf-isotope evolution of ϵHf against age for the Cape Spencer dykes (this study). The evolutionary arrays for 1000 Ma and 1600 Ma crust with average upper crustal $^{176}\text{Lu}/^{177}\text{Hf}$ values of 0.015 (Griffin *et al.* 2002). Depleted mantle evolution curve from Griffin *et al.* (2000). Hf-zircon analyses from the South Mountain Batholith (Bickerton *et al.* 2022) and the Caledonia terrane (Pollock *et al.* 2022) are also shown. (b) Nd-isotope evolution of ϵNd against age for the Cape Spencer dykes (this study). Additional ϵNd data are from the Sebago Batholith and granitic pegmatites from the Topsham area (Tomascak *et al.* 1996a, 1998), the German Bank Pluton (Pe-Piper & Jansa, 1999; Pe-Piper *et al.* 2010), the South Mountain Batholith (Clarke *et al.* 1988, 2004; Erdmann *et al.* 2009; MacDonald & Clarke, 2017), Devonian Plutons (Whalen *et al.* 1994, 1996; Mohammadi *et al.* 2020), Silurian Plutons (Whalen *et al.* 1994) and the Caledonia terrane (Samson *et al.* 2000; Whalen *et al.* 1994). Field (green-shaded) for Avalonia from Nance & Murphy (1996). Depleted mantle evolution curve from DePaolo (1981).

a hydrothermal event similar to those just mentioned. Additionally, these dykes display sharp contacts with their host rocks, without alteration haloes. There is no further evidence of ongoing hydrothermal activity affecting the host rocks after the event responsible for the ductile to brittle fabrics related to gold mineralization with cooling ages of ~ 277 Ma (Watters, 1993).

5.d. Isotopic signature

Previous studies in the Caledonia terrane and Avalonia mainly focused on whole-rock Sm-Nd of volcanic and plutonic rocks

(Whalen *et al.* 1994; Samson *et al.* 2000); therefore, there are few studies involving the use of Lu-Hf-isotope data. Available Lu-Hf analyses from Avalonia rocks are restricted to limited published *in situ* Lu-Hf-isotope data (Willner *et al.* 2013; Pollock *et al.* 2015, 2022). The first study including *in situ* zircon Lu-Hf data from Avalonia in New Brunswick, i.e. the Caledonia terrane, showed a range of ϵHf (+4.3 to +7.8) for samples from the Broad River Group and comagmatic plutons and ϵHf values between +2.1 to +8.5 for the Coldbrook Group and comagmatic plutons; these data were interpreted to show mixing of juvenile and mantle-derived magma, in addition to other crustal sources with variable Hf isotopic compositions (Pollock *et al.* 2022). Bickerton *et al.* (2022) concluded that the zircon ϵ (-2.99 to +1.68) signatures from the SMB indicated a metasomatized mantle source followed by contamination of both rocks of an underlying Avalonian terrane and metasedimentary rocks of the Meguma terrane. The narrow range of negative ϵHf values of the dykes lies on a Hf evolution trajectory typical to rocks of the South Mountain Batholith (Meguma Terrane), the Broad River Group and the Coldbrook Group (Caledonia terrane) (Figure 12(a)). The vertical trajectory in the plot of the Cape Spencer samples implies significant recycling of an evolved crustal component.

The ϵNd values for the Cape Spencer dykes plot outside the envelope for crustal-derived Avalonian rocks (Figure 12(b)), thought to be the result of repeated melting events with a common basement source (Nance & Murphy, 1996; Murphy & Nance, 2002), in contrast to the Devonian and Silurian plutons of southern New Brunswick and the Neoproterozoic intrusions in the Caledonia terrane. The dykes also show a stronger negative Nd isotopic composition than the Sebago Batholith and its associated leucogranites and aplites and the granitic pegmatites from the Topsham area (Maine, USA). These granitic pegmatites have crystallization ages ca. 270–273 Ma (Tomascak *et al.* 1996b, 1998), virtually the same ages as the Cape Spencer dykes, and therefore emplaced during the Alleghanian orogeny (Bradley *et al.* 2016). A couple of samples from Cape Spencer lie on hypothetical growth lines to a segment of the most negative ϵNd values of the SBM; a compilation of relevant Nd isotopic work on rocks from the South Mountain Batholith (Clarke *et al.* 1988, 2004; Erdmann *et al.* 2009; MacDonald & Clarke, 2017) reveals a large variation in $\epsilon\text{Nd}_{(380\text{ Ma})}$ with most data concentrated in the -7 to +0.1 range. Clarke *et al.* (1988) indicated, based on his Nd isotopic data, that the SBM had been generated by either melting of deep metasedimentary crustal material or by mixing of crustal materials with mantle-derived magma. The low ϵNd values ($\epsilon\text{Nd}_{(300\text{ Ma})} = -12.6$ to -8.6) of the German Bank Pluton, more negative than those from the dykes, are comparable with Meguma metasedimentary rocks, indicating assimilation of sediments derived from the basement beneath the southwestern Scotian Shelf (Pe-Piper & Jansa, 1999). Pe-Piper *et al.* (2010) interpreted the resulting isotopic signature in addition to the Paleoproterozoic model ages as a derivation of mixing magma of mantle origin with lower crustal melts.

5.e. Tectonic significance

In the northern Appalachians, the dextral-oblique Alleghanian collision between Laurentia and Gondwana (Hatcher, 2002; Murphy *et al.* 2011; Waldron *et al.* 2015, 2019) had started by at least 330 Ma and continued into the middle Permian, i.e. ca. 260 Ma (Nance & Linnemann, 2008; Nance *et al.* 2012; van Staal & Barr, 2012). Although limited, Alleghanian orogenesis in the United States section of the northern Appalachians included high-

grade metamorphism and associated magmatism that took place in the late Pennsylvanian and early Permian (Tomaschak *et al.* 1996a, 1996b; Walsh *et al.* 2007). In the Canadian section of the northern Appalachians, Alleghanian magmatism is restricted to the German Bank Pluton (Pe-Piper *et al.* 2010; van Staal & Barr, 2012).

The input of mantle-derived material has already been described for the German Bank Pluton (Pe-Piper *et al.* 2010) and the South Mountain Batholith (Bickerton *et al.* 2022). From the Hf-Nd-isotope analyses, there is no indication of the involvement or mixing of mantle material for the Cape Spencer dykes, as those strong negative Nd values and the negative Hf values point to assimilation and reworking of old crust instead of a juvenile source.

Isotopic data from the Cape Spencer aplitic textured leucogranitic dykes show compositional ranges of whole-rock $\epsilon\text{Nd}_{(274 \text{ Ma})}$ values from -9.7 to -5.7 , $\epsilon\text{Hf}_{(274 \text{ Ma})}$ from -1.8 to -1.0 and whole-rock Nd model ages (T_{DM}) from 1.3 to 1.6 Ga. These isotopic characteristics suggest that the dykes are derived from the crystalline residuum of the magmas resulting from the partial melting of crustal source rocks that, while ascending, became contaminated with Meguma metasedimentary rocks and/or Avalonian sedimentary rocks. Continued subduction of the Rheic Ocean displaying an ongoing zipper-style closure derived in the Alleghanian collision of Gondwana with the Appalachian part of Laurentia (Kroner *et al.* 2022); this process could have led to partial melting of the underthrust Avalonian basement, currently extending 50 km south of the surface suture (Pe-Piper & Jansa, 1999), under Meguma. Melt emplacement would be confined to favourable channels as faults, in this case, the MFZ with continued dextral-strike-slip motion during the Pennsylvanian-Permian (Murphy *et al.* 2011; Waldron *et al.* 2015). With such an active environment, the fracturing of solid rocks will allow the extraction or ascent of evolved low T, carbonate-bearing granitic melt by the movement of the silicic parental melt.

6. Conclusions

The low T leucogranitic dykes show major and trace elements similar to those of I-type granitoids, although they exhibit evidence of autometamorphic albittization, but have igneous calcite. These dykes have an age of 273.7 ± 1.3 Ma, based on U-Pb dating of monazite and constitute the youngest magmatic event in southern New Brunswick to this date. The emplacement of these dykes provides a lower age constraint for the gold mineralization in the area, as they crosscut the various deformation fabrics of the host rocks to which gold deposition is related.

Nd-Hf isotopic signatures do not suggest the input of mantle-derived material for the dykes from the Cape Spencer area; instead, they point towards partial melting of a crustal source with assimilation of Meguma metasedimentary rocks and/or Avalonian sedimentary rocks. Important geodynamic events occurred during the Alleghanian orogeny with the continued subduction of the Rheic Ocean under composite Laurentia that provided the heat supply and material sources for these partial melts to form and ascend and be emplaced as aplitic dykes quenched due to depressurization associated with emplacement. The activation of deep crustal faults in response to the strike-slip motion that was taking place along the MFZ could have provided the means for the ascent of these low-T crustal melts.

Supplementary material. To view supplementary material for this article, please visit <https://doi.org/10.1017/S0016756824000141>

Acknowledgements. We want to thank Brandon Boucher (UNB) for assistance with LA-ICP-MS analysis. Dr. Shuangquan Zhang (Carleton University) is thanked for the help and supervision of Nd-Hf isotopic measurements. SEM work and BSE imaging were carried out with the help of Dr. Douglas Hall and Steven R. Cogswell (UNB). The authors acknowledge Dr. Georgia Pe-Piper and two anonymous reviewers for the meticulous and constructive reviews of the manuscript.

Financial support. Project was variably funded by the New Brunswick Department of Natural Resources and Energy Development and New Brunswick Innovation Foundation.

Competing interests. The authors declare none.

References

- Arevalo R and McDonough WF (2010) Chemical variations and regional diversity observed in MORB. *Chemical Geology* **271**, 70–85.
- Artemieva IM, Thybo H, Jakobsen K, Sørensen NK and Nielsen LSK (2017) Heat production in granitic rocks: Global analysis based on a new data compilation GRANITE2017. *Earth-Science Reviews* **172**, 1–26.
- Audétat A, Pettke T and Dolejš D (2004) Magmatic anhydrite and calcite in the ore-forming quartz-monzodiorite magma at Santa Rita, New Mexico (USA): Genetic constraints on porphyry-Cu mineralization. *Lithos* **72**, 147–161.
- Ballouard C, Massuyeau M, Elburg MA, Tappe S, Viljoen F and Brandenburg, JT (2020) The magmatic and magmatic-hydrothermal evolution of felsic igneous rocks as seen through Nb-Ta geochemical fractionation, with implications for the origins of rare-metal mineralizations. *Earth-Science Reviews* **203**, 103115.
- Ballouard C, Poujol M, Boulvais P, Branquet Y, Tartèse R and Vigneresse JL (2016) Nb-Ta fractionation in peraluminous granites: A marker of the magmatic-hydrothermal transition. *Geology* **44**, 231–234.
- Barr SM, Johnson SC, Dunning GR, White CE, Park AF, Wälle M and Langille A (2020) New Cryogenian, Neoproterozoic, and middle Paleozoic U–Pb zircon ages from the Caledonia terrane, southern New Brunswick, Canada: Better constrained but more complex volcanic stratigraphy. *Atlantic Geoscience* **56**, 163–187.
- Barr SM, van Rooyen D, Miller BV, White CE and Johnson SC (2019). Detrital zircon signatures in Precambrian and Paleozoic sedimentary units in southern New Brunswick – more pieces of the puzzle. *Atlantic Geoscience* **55**, 275–322.
- Barr SM and White CE (1996a). Contrasts in late Precambrian–early Paleozoic tectonothermal history between Avalon composite terrane *sensu stricto* and other possible peri-Gondwanan terranes in southern New Brunswick and Cape Breton Island, Canada. In *Avalonian and related peri-Gondwanan terranes of the Circum-North Atlantic* (eds RD Nance and MD Thompson), pp. 95–108. Geological Society of America, Special Paper no. 304.
- Barr SM and White CE (1996b). Tectonic setting of Avalonian volcanic and plutonic rocks in the Caledonian Highlands, southern New Brunswick, Canada. *Canadian Journal of Earth Sciences* **33**, 156–168.
- Barr SM and White CE (1999) Field Relations, Petrology and Structure of Neoproterozoic Rocks in the Caledonian Highlands, Southern New Brunswick. Geological Survey of Canada Bulletin, Bulletin 530, 101 pp.
- Bau M (1996) Controls on the fractionation of isovalent trace elements in magmatic and aqueous systems: Evidence from Y/Ho, Zr/Hf, and lanthanide tetrad effect. *Contributions to Mineralogy and Petrology* **123**, 323–333.
- Bea F (1996) Residence of REE, Y, Th and U in Granites and Crustal Protoliths; implications for the chemistry of crustal melts. *Journal of Petrology* **37**, 521–552.
- Bea F, Mazhari A, Montero P, Amimi S and Ghalamghash J (2011) Zircon dating, Sr and Nd isotopes, and element geochemistry of the Khalifan pluton, NW Iran: Evidence for Variscan magmatism in a supposedly Cimmerian superterrane. *Journal of Asian Earth Sciences* **40**, 172–179.
- Bickerton L, Kontak DJ, Murphy JB, Kellett DA, Samson IM, Marsh JH, Dunning G and Stern R (2022) The age and origin of the South Mountain Batholith (Nova Scotia, Canada) as constrained by zircon U–Pb

- geochronology, geochemistry, and O–Hf isotopes. *Canadian Journal of Earth Sciences* **59**, 418–454.
- Boehnke P, Watson EB, Trail D, Harrison TM and Schmitt AK** (2013) Zircon saturation re-revisited. *Chemical Geology* **351**, 324–334.
- Bradley D, Shea E, Buchwaldt R, Bowring S, Benowitz J, O’Sullivan P and McCauley A** (2016) Geochronology and tectonic context of lithium–cesium–tantalum pegmatites in the Appalachians. *The Canadian Mineralogist* **54**, 945–969.
- Brown M** (2013) Granite: From genesis to emplacement. *GSA Bulletin* **125**, 1079–1113.
- Champion DC and Chappell BW** (1992) Petrogenesis of felsic I-type granites: An example from northern Queensland. *Earth and Environmental Science Transactions of The Royal Society of Edinburgh* **83**, 115–126.
- Chappell BW and White AJR** (2001) Two contrasting granite types: 25 years later. *Australian Journal of Earth Sciences* **48**, 489–499.
- Chappell BW, White AJR, Williams IS and Wyborn D** (2004) Low- and high-temperature granites. *Earth and Environmental Science Transactions of The Royal Society of Edinburgh* **95**, 125–140.
- Clarke DB and Halliday AN** (1985) Sm/Nd isotopic investigation of the age and origin of the Meguma Zone metasedimentary rocks. *Canadian Journal of Earth Sciences* **22**, 102–107.
- Clarke DB, Halliday AN and Hamilton PJ** (1988) Neodymium and strontium isotopic constraints on the origin of the peraluminous granitoids of the South Mountain Batholith, Nova Scotia, Canada. *Chemical Geology* **73**, 15–24.
- Clarke DB, MacDonald MA and Erdmann S** (2004) Chemical variation in Al_2O_3 –CaO–Na₂O–K₂O space: Controls on the peraluminosity of the South Mountain Batholith. *Canadian Journal of Earth Sciences* **41**, 785–798.
- Clarke DB, MacDonald MA and Tate MC** (1997) Late Devonian mafic-felsic magmatism in the Meguma Zone, Nova Scotia. In *The Nature of Magmatism in the Appalachian Orogen* (eds AK Sinha, JB Whalen and JP Hogan), pp. 107–127. Geological Society of America, GSA Memoirs 191.
- Cousens BL** (1996) Magmatic evolution of Quaternary mafic magmas at Long Valley Caldera and the Devils Postpile, California: Effects of crustal contamination on lithospheric mantle-derived magmas. *Journal of Geophysical Research: Solid Earth* **101**, 27673–27689.
- Culshaw N and Reynolds P** (1997) ⁴⁰Ar/³⁹Ar age of shear zones in the southwest Meguma Zone between Yarmouth and Meteghan, Nova Scotia. *Canadian Journal of Earth Sciences* **34**, 848–853.
- De la Roche H, Leterrier J, Grandclaude P and Marchal M** (1980) A classification of volcanic and plutonic rocks using R1R2-diagram and major-element analyses—Its relationships with current nomenclature. *Chemical Geology* **29**, 183–210.
- DePaolo DJ** (1981) Neodymium isotopes in the Colorado Front Range and crust–mantle evolution in the Proterozoic. *Nature* **291**, 193–196.
- Dunning GR, Barr SM, Giles PS, McGregor DC, Pe-Piper G and Piper DJ** (2002) Chronology of Devonian to early Carboniferous rifting and igneous activity in southern Magdalen Basin based on U–Pb (zircon) dating. *Canadian Journal of Earth Sciences* **39**, 1219–1237.
- Erdmann S, Jamieson RA and MacDonald MA** (2009) Evaluating the origin of garnet, cordierite, and biotite in granitic rocks: A case study from the South Mountain Batholith, Nova Scotia. *Journal of Petrology* **50**, 1477–1503.
- Ersay I, Greenough JD, Larson KP and Dostal J** (2022) Zircon reveals multistage, magmatic and hydrothermal Rare Earth Element mineralization at Debert Lake, Nova Scotia, Canada. *Ore Geology Reviews* **144**, 104780.
- Förster HJ, Tischendorf G and Trumbull RB** (1997) An evaluation of the Rb vs. (Y + Nb) discrimination diagram to infer tectonic setting of silicic igneous rocks. *Lithos* **40**, 261–293.
- Fyffe LR, Johnson SC and van Staal CR** (2011) A review of Proterozoic to early Paleozoic Lithotectonic Terranes in New Brunswick, Canada and their Tectonic Evolution during Penobscot, Taconic, Salinic and Acadian Orogenesis. *Atlantic Geoscience* **47**, 211–248.
- Green TH** (1995) Significance of Nb/Ta as an indicator of geochemical processes in the crust–mantle system. *Chemical Geology* **120**, 347–359.
- Griffin WL, Pearson NJ, Belousova E, Jackson SE, van Acherbergh E, O’Reilly SY and Shee SR** (2000) The Hf isotope composition of cratonic mantle: LAM-MC-ICPMS analysis of zircon megacrysts in kimberlites. *Geochimica et Cosmochimica Acta* **64**, 133–147.
- Griffin WL, Wang X, Jackson SE, Pearson NJ, O’Reilly SY, Xu X and Zhou X** (2002) Zircon chemistry and magma mixing, SE China: In-situ analysis of Hf isotopes, Tonglu and Pingtan igneous complexes. *Lithos* **61**, 237–269.
- Harrison TM, Watson EB and Aikman AB** (2007) Temperature spectra of zircon crystallization in plutonic rocks. *Geology* **35**, 635–638.
- Hasterok D, Gard M and Webb J** (2018) On the radiogenic heat production of metamorphic, igneous, and sedimentary rocks. *Geoscience Frontiers* **9**, 1777–1794.
- Hatcher RD** (2002) Alleghanian (Appalachian) orogeny, a product of zipper tectonics: Rotational transpressive continent–continent collision and closing of ancient oceans along irregular margins. In *Variscan–Appalachian dynamics: The building of the late Paleozoic basement* (eds JRM Catalán, RD Hatcher Jr, R Arenas and FD García), pp. 199–208. Geological Society of America, Special Paper 364.
- Hatcher RD** (2005) North America: Southern and Central Appalachians. In *Encyclopedia of Geology* (eds RC Selley, LRM Cocks and IR Plimer), pp. 72–81: Elsevier Academic Press, UK.
- Hatcher RD** (2010) The Appalachian orogen: A brief summary. In *From Rodinia to Pangea: The Lithotectonic Record of the Appalachian Region* (eds RP Tollo, MJ Bartholomew, JP Hibbard and PM Karabinos), pp. 1–19. Geological Society of America, GSA Memoirs 206.
- Hibbard JP, van Staal CR and Miller BV** (2007a) Links among Carolina, Avalonia, and Ganderia in the Appalachian peri-Gondwanan realm. In *Whence the Mountains? Inquiries into the Evolution of Orogenic Systems: A Volume in Honor of Raymond A. Price* (eds JW Sears, TA Harms and CA Evenchick), pp. 291–311: Geological Society of America, Special Paper 433.
- Hibbard JP, van Staal CR and Rankin DW** (2007b) A comparative analysis of pre-Silurian crustal building blocks of the northern and the southern Appalachian orogen. *American Journal of Science* **307**, 23–45.
- Hibbard JP, van Staal CR and Rankin DW** (2010) Comparative analysis of the geological evolution of the northern and southern Appalachian orogen: Late Ordovician–Permian. In *From Rodinia to Pangea: The Lithotectonic Record of the Appalachian Region* (eds RP Tollo, MJ Bartholomew, JP Hibbard and PM Karabinos), pp. 51–69. Geological Society of America, GSA Memoirs 206.
- Hildebrand RS and Whalen JB** (2014) Arc and Slab-Failure Magmatism in Cordilleran Batholiths II – The Cretaceous Peninsular Ranges Batholith of Southern and Baja California. *Geoscience Canada* **41**, 399–458.
- Hildebrand RS and Whalen JB** (2017) *The Tectonic Setting and Origin of Cretaceous Batholiths within the North American Cordillera: The Case for Slab Failure Magmatism and Its Significance for Crustal Growth*. Geological Society of America, Special Paper 532, 88 pp.
- Hofmann AW** (1988) Chemical differentiation of the Earth: The relationship between mantle, continental crust, and oceanic crust. *Earth and Planetary Science Letters* **90**, 297–314.
- Holloway JR** (1976) Fluids in the evolution of granitic magmas: Consequences of finite CO₂ solubility. *GSA Bulletin* **87**, 1513–1518.
- Jochum KP, Seufert HM, Spettel B and Palme H** (1986) The solar-system abundances of Nb, Ta, and Y, and the relative abundances of refractory lithophile elements in differentiated planetary bodies. *Geochimica et Cosmochimica Acta* **50**, 1173–1183.
- Johnson SC and Rossiter SL** (2022) Update on bedrock mapping in the Caledonian Highlands, southeastern New Brunswick. In *Geoscience Project Summaries and Other Activities 2019* (ed EA Keith), pp. 50–54. New Brunswick Department of Energy and Resource Development, Information Circular 2022-1.
- Jutras P, Prichonnet G and McCutcheon S** (2003) Alleghanian deformation in the eastern Gaspé Peninsula of Quebec, Canada. *GSA Bulletin* **115**, 1538–1551.
- Kelley KA and Cottrell E** (2009) Water and the oxidation state of subduction zone magmas. *Science* **325**, 605–607.
- Kerr A, Jenner GA and Fryer BJ** (1995) Sm–Nd isotopic geochemistry of Precambrian to Paleozoic granitoid suites and the deep-crustal structure of the southeast margin of the Newfoundland Appalachians. *Canadian Journal of Earth Sciences* **32**, 224–245.
- Kontak DJ, Ansdell K and Archibald DA** (2000) Zn–Pb mineralization associated with a mafic dyke at Cheverie, Hants County, Nova Scotia: implications for Carboniferous metallogeny. *Atlantic Geoscience* **36**, 7–26.

- Kontak DJ, Archibald DA, Creaser RA and Heaman LM** (2008) Dating hydrothermal alteration and IOCG mineralization along a terrane-bounding fault zone: the Copper Lake deposit, Nova Scotia. *Atlantic Geoscience* **44**, 146–166.
- Koukouvelas I, Pe-Piper G and Piper DJW** (2002) The role of dextral transpressional faulting in the evolution of an early Carboniferous mafic-felsic plutonic and volcanic complex: Cobequid Highlands, Nova Scotia, Canada. *Tectonophysics* **348**, 219–246.
- Kroner U, Stephan T and Romer RL** (2022) Paleozoic orogenies and relative plate motions at the sutures of the Iapetus-Rheic Ocean. In *New Developments in the Appalachian-Caledonian-Variscan Orogen* (eds YD Kuiper, JB Murphy, RD Nance, RA Strachan and MD Thompson), pp. 1–23. Geological Society of America, GSA Special Paper 504.
- Landing E** (1996) Avalon: Insular continent by the latest Precambrian. In *Avalonian and related peri-Gondwanan terranes of the Circum-North Atlantic* (eds RD Nance and MD Thompson), pp. 29–63. Geological Society of America, Special Paper no. 304
- MacDonald MA and Clarke DB** (2017) Occurrence, origin, and significance of melagranites in the South Mountain Batholith, Nova Scotia. *Canadian Journal of Earth Sciences* **54**, 693–713.
- MacHattie TG and O'Reilly GA** (2008) Timing of iron oxide-copper-gold (IOCG) mineralization and alteration along the Cobequid-Chedabucto Fault Zone. In *Mineral Resources Branch Report of Activities 2008* (eds DR MacDonald and KA Mills), pp. 63–69. Nova Scotia Department of Natural Resources, Report ME 2009-1.
- Malay BC, Braid JA, Archibald DB and McFarlane CRM** (2023) Depositional environment and provenance of Early Carboniferous clastic sedimentary rocks at McIsaacs Point, Nova Scotia: Implications for syntectonic basin development during the formation of Pangaea. *Geological Society, London, Special Publications* **531**, 323–344.
- Maniar PD and Piccoli P** (1989) Tectonic discrimination of granitoids. *GSA Bulletin* **101**, 635–643.
- McDonough WF and Sun SS** (1995) The composition of the Earth. *Chemical Geology* **120**, 223–253.
- Miller CF, McDowell SM and Mapes RW** (2003) Hot and cold granites? Implications of zircon saturation temperatures and preservation of inheritance. *Geology* **31**, 529–532.
- Mohammadi N, Lentz DR, McFarlane CRM and Cousens B** (2020) Geochemistry of the highly evolved Sn-W-Mo-bearing Mount Douglas Granite, New Brunswick, Canada: Implications for origin and mineralization. *Ore Geology Reviews* **117**, 103266.
- Montel JM** (1993) A model for monazite/melt equilibrium and application to the generation of granitic magmas. *Chemical Geology* **110**, 127–146.
- Murphy JB and Collins AS** (2008) ⁴⁰Ar–³⁹Ar white mica ages reveal Neoproterozoic/Paleozoic provenance and an Alleghanian overprint in coeval Upper Ordovician–Lower Devonian rocks of Meguma and Avalonia. *Tectonophysics* **461**, 265–276.
- Murphy JB and Keppie JD** (1998) Late Devonian palinspastic reconstruction of the Avalon-Meguma terrane boundary: Implications for terrane accretion and basin development in the Appalachian orogen. *Tectonophysics* **284**, 221–231.
- Murphy JB and Nance RD** (2002) Sm-Nd isotopic systematics as tectonic tracers: An example from West Avalonia in the Canadian Appalachians. *Earth-Science Reviews* **59**, 77–100.
- Murphy JB, Waldron JWF, Kontak DJ, Pe-Piper G and Piper DJW** (2011) Minas Fault Zone: Late Paleozoic history of an intra-continental orogenic transform fault in the Canadian Appalachians. *Journal of Structural Geology* **33**, 312–328.
- Nance RD** (1986) Late Carboniferous Tectonostratigraphy in the Avalon Terrane of Southern New Brunswick. *Atlantic Geoscience* **22**, 308–326.
- Nance RD** (1987) Dextral Transpression and Late Carboniferous Sedimentation in the Fundy Coastal Zone of Southern New Brunswick. *Sedimentary Basins and Basin-Forming Mechanisms* **12**, 363–377.
- Nance RD, Gutiérrez-Alonso G, Keppie JD, Linnemann U, Murphy JB, Quesada C, Strachan RA and Woodcock NH** (2012) A brief history of the Rheic Ocean. *Geoscience Frontiers* **3**, 125–135.
- Nance RD and Linnemann U** (2008) The Rheic Ocean: Origin, evolution, and significance. *GSA Today* **18**, 4–12.
- Nance RD and Murphy JB** (1996) Basement isotopic signatures and Neoproterozoic paleogeography of Avalonian-Cadomian and related terranes in the Circum-North Atlantic. In *Avalonian and related peri-Gondwanan terranes of the Circum-North Atlantic* (eds RD Nance and MD Thompson), pp. 333–346. Geological Society of America, Special Paper no. 304
- Nance RD and Warner JB** (1986) Variscan tectonostratigraphy of the Mispic Group, southern New Brunswick: Structural geometry and deformational history. In *Current Research Part A*, pp. 351–358. Geological Survey of Canada, Paper 86-1A.
- Park AF and Hinds SJ** (2020) Structure and stratigraphy in the Pennsylvanian tectonic zone of southern New Brunswick, Canada: The 'Maritime coastal disturbance' revisited. In *Pannotia to Pangaea: Neoproterozoic and Paleozoic Orogenic Cycles in the Circum-Atlantic Region* (eds JB Murphy, RA Strachan, C Quesada), pp. 443–468. Geological Society, London, Special Publications 503.
- Park AF, Treat RL, Barr SM, White CE, Miller BV, Reynolds PH and Hamilton MA** (2014) Structural setting and age of the Partridge Island block, southern New Brunswick, Canada: A link to the Cobequid Highlands of northern mainland Nova Scotia. *Canadian Journal of Earth Sciences* **51**, 1–24.
- Pe-Piper G and Jansa LF** (1999) Pre-Mesozoic basement rocks offshore Nova Scotia, Canada: New constraints on the accretion history of the Meguma terrane. *GSA Bulletin* **111**, 1773–1791.
- Pe-Piper G, Kamo SL and McCall C** (2010) The German Bank pluton, offshore SW Nova Scotia: Age, petrology, and regional significance for Alleghanian plutonism. *GSA Bulletin* **122**, 690–700.
- Pe-Piper G and Piper DJW** (2021) Controls on barite mineralization in a major intracontinental shear zone: Carboniferous of the Cobequid Highlands, Nova Scotia. *Minerals* **11**, 1413.
- Pe-Piper G, Piper DJW, McFarlane CRM, Sangster C, Zhang Y and Boucher B** (2018) Petrology, chronology and sequence of vein systems: Systematic magmatic and hydrothermal history of a major intracontinental shear zone, Canadian Appalachians. *Lithos* **304–307**, 298–310.
- Pearce J** (1996) Sources and settings of granitic rocks. *Episodes Journal of International Geoscience* **19**, 120–125.
- Pearce J, Harris NBW and Tindle AG** (1984) Trace element discrimination diagrams for the tectonic interpretation of granitic rocks. *Journal of Petrology* **25**, 956–983.
- Pfänder JA, Münker C, Stracke A and Mezger K** (2007) Nb/Ta and Zr/Hf in ocean island basalts—Implications for crust–mantle differentiation and the fate of Niobium. *Earth and Planetary Science Letters* **254**, 158–172.
- Pollock JC, Barr SM, van Rooyen D and White CE** (2022) Insights from Lu-Hf zircon isotopic data on the crustal evolution of Avalonia and Ganderia in the northern Appalachian orogen. In *New Developments in the Appalachian-Caledonian-Variscan Orogen* (eds YD Kuiper, JB Murphy, RD Nance, RA Strachan and MD Thompson), pp. 173–207. Geological Society of America, GSA Special Paper 504.
- Pollock JC, Sylvester PJ and Barr SM** (2015) Lu-Hf zircon and Sm-Nd whole-rock isotope constraints on the extent of juvenile arc crust in Avalonia: Examples from Newfoundland and Nova Scotia, Canada. *Canadian Journal of Earth Sciences* **52**, 161–181.
- Ravenhurst CE, Reynolds PH, Zentilli M, Krueger HW and Blenkinsop J** (1989) Formation of Carboniferous Pb-Zn and barite mineralization from basin-derived fluids, Nova Scotia, Canada. *Economic Geology* **84**, 1471–1488.
- Reynolds PH, Pe-Piper G and Piper DJW** (2012) Detrital muscovite geochronology and the Cretaceous tectonics of the inner Scotian Shelf, southeastern Canada. *Canadian Journal of Earth Sciences* **49**, 1558–1566.
- Richard R** (2005) Mineralogical and geochemical examination of the gold mineralization within the Silica Zone and Open Pit at Cape Spencer, New Brunswick. BSc thesis, University of New Brunswick.
- Ross PS and Bédard JH** (2009) Magmatic affinity of modern and ancient subalkaline volcanic rocks determined from trace-element discriminant diagrams. *Canadian Journal of Earth Sciences* **46**, 823–839.
- Rudnick RL and Gao S** (2014) Composition of the Continental Crust. In *Treatise on Geochemistry (Second Edition)* (eds HD Holland and KK Turekian), pp. 1–51. Elsevier.
- Ruitenberg AA** (1995) Metallogeny: Syn- and post-accretion structurally controlled mesothermal/epithermal mineralization. In *Geology of the*

- Appalachian-Caledonian Orogen in Canada and Greenland* (ed H Williams), pp. 751–754. Geological Survey of Canada, Geology of Canada no. 6.
- Samson SD, Barr SM and White CE** (2000) Nd isotopic characteristics of terranes within the Avalon Zone, southern New Brunswick. *Canadian Journal of Earth Sciences* **37**, 1039–1052.
- Samson SD, Coler DG and Speer JA** (1995) Geochemical and Nd-Sr-Pb isotopic composition of Alleghanian granites of the southern Appalachians: Origin, tectonic setting, and source characterization. *Earth and Planetary Science Letters* **134**, 359–376.
- Scharfenberg L, Regelous A and Wall HD** (2019) Radiogenic heat production of Variscan granites from the Western Bohemian Massif, Germany. *Journal of Geosciences* **64**, 251–259.
- Siégl C, Bryan SE, Allen CM and Gust DA** (2018) Use and abuse of zircon-based thermometers: A critical review and a recommended approach to identify antecrystic zircons. *Earth-Science Reviews* **176**, 87–116.
- Speer JA and Hoff KW** (1997) Elemental composition of the Alleghanian granitoid plutons of the southern Appalachians. In *The Nature of Magmatism in the Appalachian Orogen* (eds AK Sinha, JB Whalen and JP Hogan), pp. 287–308. Geological Society of America, GSA Memoirs 191.
- Sun S and McDonough WF** (1989). Chemical and isotopic systematics of oceanic basalts: Implications for mantle composition and processes. In *Magmatism in the Ocean Basins* (eds AD Saunders and MJ Norry), 1pp. 313–345. Geological Society, London, Special Publications 42.
- Swanson SE** (1979) The effect of CO₂ on phase equilibria and crystal growth in the system KAlSi₃O₈-NaAlSi₃O₈-CaAl₂Si₂O₈-SiO₂-H₂O-CO₂ to 8000 bars. *American Journal of Science* **279**, 703–720.
- Tang M, Lee CTA, Chen K, Erdman M, Costin G and Jiang H** (2019) Nb/Ta systematics in arc magma differentiation and the role of arclogites in continent formation. *Nature Communications* **10**, 235.
- Tanoli SK and Pickerill RK** (1988) Lithostratigraphy of the Cambrian – Lower Ordovician Saint John Group, southern New Brunswick. *Canadian Journal of Earth Sciences* **25**, 669–690.
- Tartèse R and Boulvais P** (2010) Differentiation of peraluminous leucogranites “en route” to the surface. *Lithos* **114**, 353–368.
- Taylor SR and McLennan SM** (1985) *The continental crust: Its composition and evolution*. Oxford: Blackwell Scientific, 312 pp.
- Taylor SR and McLennan SM** (1995) The geochemical evolution of the continental crust. *Reviews of Geophysics* **33**, 241–265.
- Tomascaq PB, Krogstad EJ and Walker RJ** (1996a) Nature of the crust in Maine, USA: Evidence from the Sebago batholith. *Contributions to Mineralogy and Petrology* **125**, 45–59.
- Tomascaq PB, Krogstad EJ and Walker RJ** (1996b) U-Pb Monazite Chronology of Granitic Rocks from Maine: Implications for Late Paleozoic Tectonics in the Northern Appalachians. *The Journal of Geology* **104**, 185–195.
- Tomascaq PB, Krogstad EJ and Walker RJ** (1998) Sm-Nd isotope systematics and the derivation of granitic pegmatites in southwestern Maine. *The Canadian Mineralogist* **36**, 327–337.
- van Staal CR** (2007) Pre-Carboniferous tectonic evolution and metallogeny of the Canadian Appalachians. In *Mineral deposits of Canada: A synthesis of major deposit-types, district metallogeny, the evolution of geological provinces, and exploration methods* (ed WD Goodfellow), pp. 793–818. Geological Association of Canada, Mineral Deposits Division, Special Publication No. 5.
- van Staal CR and Barr SM** (2012) Lithospheric architecture and tectonic evolution of the Canadian Appalachians. In *Tectonic Styles in Canada: The LITHOPROBE perspective* (eds JA Percival, FA Cook and RM Clowes), pp. 41–95. Geological Association of Canada, Special Paper 49.
- van Staal CR, Barr SM, Waldron JWF, Schofield DI, Zagorevski A and White CE** (2021) Provenance and Paleozoic tectonic evolution of Ganderia and its relationships with Avalonia and Megumia in the Appalachian-Caledonide orogen. *Gondwana Research* **98**, 212–243.
- Vermeesch P and Pease V** (2021) A genetic classification of the tholeiitic and calc-alkaline magma series. *Geochemical Perspectives Letters* **19**, 1–6.
- Villasca C, Barbero L and Rogers G** (1998) Crustal origin of Hercynian peraluminous granitic batholiths of Central Spain: Petrological, geochemical and isotopic (Sr, Nd) constraints. *Lithos* **43**, 55–79.
- Waldron JWF, Barr SM, Park AF, White CE and Hibbard J** (2015) Late Paleozoic strike-slip faults in Maritime Canada and their role in the reconfiguration of the northern Appalachian orogen. *Tectonics* **34**, 1661–1684.
- Waldron JWF, McCausland PJA, Barr SM, Schofield DI, Reusch D and Wu L** (2022) Terrane history of the Iapetus Ocean as preserved in the northern Appalachians and western Caledonides. *Earth-Science Reviews* **233**, 104163.
- Waldron JWF, Schofield DI and Murphy JB** (2019) Diachronous Paleozoic accretion of peri-Gondwanan terranes at the Laurentian margin. In *Fifty Years of the Wilson Cycle Concept in Plate Tectonics* (eds RW Wilson, GA Houseman, KJW McCaffrey, AG Doré and SJH Buiters), pp. 289–310. Geological Society, London, Special Publications 470.
- Waldron JWF, White CE, Barr SM, Simonetti A and Heaman LM** (2009) Provenance of the Meguma terrane, Nova Scotia: Rifted margin of early Paleozoic Gondwana. *Canadian Journal of Earth Sciences* **46**, 1–8.
- Walsh GJ, Aleinikoff JN and Wintsch RP** (2007) Origin of the Lyme Dome and implications for the timing of multiple Alleghanian deformational and intrusive events in southern Connecticut. *American Journal of Science* **307**, 168–215.
- Warner JB** (1985) Variscan fabrics and structural geometry of the Mispec-Cape Spencer region, Saint John, New Brunswick. MSc thesis, Ohio University.
- Watson EB and Harrison TM** (1983) Zircon saturation revisited: Temperature and composition effects in a variety of crustal magma types. *Earth and Planetary Science Letters* **64**, 295–304.
- Watters SE** (1993) Structure and alteration related to Hercynian gold deposition, Cape Spencer, New Brunswick, Canada. PhD thesis, University of Western Ontario.
- Whalen JB, Fyffe LR, Longstaffe FJ and Jenner GA** (1996) The position and nature of the Gander–Avalon boundary, southern New Brunswick, based on geochemical and isotopic data from granitoid rocks. *Canadian Journal of Earth Sciences* **33**, 129–139.
- Whalen JB and Hildebrand RS** (2019) Trace element discrimination of arc, slab failure, and A-type granitic rocks. *Lithos* **348–349**, 105179.
- Whalen JB, Jenner GA, Currie KL, Barr SM, Longstaffe FJ and Hegner E** (1994) Geochemical and Isotopic Characteristics of Granitoids of the Avalon Zone, Southern New Brunswick: Possible Evidence for Repeated Delamination Events. *The Journal of Geology* **102**, 269–282.
- White CE** (2010) Stratigraphy of the Lower Paleozoic Goldenville and Halifax groups in the western part of southern Nova Scotia. *Atlantic Geoscience* **46**, 136–154.
- White CE and Barr SM** (2010) Lithochemistry of the Lower Paleozoic Goldenville and Halifax groups, southwestern Nova Scotia, Canada: Implications for stratigraphy, provenance, and tectonic setting of the Meguma terrane. In *From Rodinia to Pangea: The Lithotectonic Record of the Appalachian Region* (eds RP Tollo, MJ Bartholomew, JP Hibbard and PM Karabinos), pp. 347–366. Geological Society of America, GSA Memoirs 206.
- White CE, Barr SM and Linnemann U** (2018) U–Pb (zircon) ages and provenance of the White Rock Formation of the Rockville Notch Group, Meguma terrane, Nova Scotia, Canada: Evidence for the “Sardian gap” and West African origin. *Canadian Journal of Earth Sciences* **55**, 589–603.
- Williams H** (1979) Appalachian Orogen in Canada. *Canadian Journal of Earth Sciences* **16**, 792–807.
- Willner AP, Barr SM, Gerdes A, Massonne HJ and White CE** (2013) Origin and evolution of Avalonia: Evidence from U–Pb and Lu–Hf isotopes in zircon from the Mira terrane, Canada, and the Stavelot–Venn Massif, Belgium. *Journal of the Geological Society* **170**, 769–784.
- Wipperfurth SA, Guo M, Šrámek O and McDonough WF** (2018) Earth’s chondritic Th/U: Negligible fractionation during accretion, core formation, and crust–mantle differentiation. *Earth and Planetary Science Letters* **498**, 196–202.
- Yang Y, Zhang H, Chu Z, Xie L and Wu F** (2010) Combined chemical separation of Lu, Hf, Rb, Sr, Sm and Nd from a single rock digest and precise and accurate isotope determinations of Lu–Hf, Rb–Sr and Sm–Nd isotope systems using Multi-Collector ICP-MS and TIMS. *International Journal of Mass Spectrometry* **290**, 120–126.
- Zheng YF** (2019) Subduction zone geochemistry. *Geoscience Frontiers* **10**, 1223–1254.